Quantum phase transitions in single-crystal $Mn_{1-x}Fe_xSi$ and $Mn_{1-x}Co_xSi$: Crystal growth, magnetization, ac susceptibility, and specific heat

A. Bauer,[1] A. Neubauer,[1] C. Franz,[1] W. Münzer,[1] M. Garst,[2,3] and C. Pfleiderer[1,*]
[1]*Physik-Department E21, Technische Universität München, James-Franck-Straße, D-85748 Garching, Germany*
[2]*Physik-Department T30, Technische Universität München, James-Franck-Straße, D-85748 Garching, Germany*
[3]*Institute for Theoretical Physics, Universität zu Köln, Zülpicher Straße 77, D-50937 Köln, Germany*
(Received 29 March 2010; revised manuscript received 1 July 2010; published 4 August 2010)

We report the magnetization, ac susceptibility, and specific heat of optically float-zoned single crystals of $Mn_{1-x}Fe_xSi$ and $Mn_{1-x}Co_xSi$ for temperatures down to ~ 2 K and magnetic fields up to 9 T. The suppression of the helimagnetic transition temperature T_1 above a critical composition x_1, as seen in the magnetization, ac susceptibility, and specific heat, suggests the existence of a quantum phase transition at x_1. A Vollhardt invariance at a temperature $T_2 > T_1$, which may be attributed to the Dzyaloshinsky-Moriya (DM) spin-orbit interactions, is also suppressed with increasing x and vanishes above a concentration x_2, where $x_2 > x_1$. When suppressing the effects of the DM interactions in an applied magnetic field, the magnetization for sufficiently large fields shares the signatures expected of an underlying putative ferromagnetic quantum critical point for a critical concentration x_c, where $x_1 < x_c < x_2$. As a function of normalized concentration x/x_c, where $x_c^{Co} \approx 0.084$ and $x_c^{Fe} \approx 0.192$, the properties of $Mn_{1-x}Fe_xSi$ and $Mn_{1-x}Co_xSi$ are essentially identical with $x_1/x_c \approx 0.78$ and $x_2/x_c \approx 1.17$. Taken together, our study identifies $Mn_{1-x}Fe_xSi$ and $Mn_{1-x}Co_xSi$ as model systems in which the influence of DM interactions on ferromagnetic quantum criticality may be studied.

DOI: 10.1103/PhysRevB.82.064404 PACS number(s): 74.40.Kb, 75.10.Lp, 74.25.Ha, 74.70.Ad

I. MOTIVATION

The experimental and theoretical investigations of quantum phase transitions in magnetic materials attract great interest as the possible origin of new types of low-lying excitations of many-body systems. Quantum phase transitions (QPTs) attract also interest as the possible origin of novel forms of electronic order. One of the most important phenomenological models that permits the identification of anomalous behavior at QPTs is the spin-fluctuation theory of weakly magnetic itinerant-electron compounds, also known as self-consistent random-phase approximation (RPA) or self-consistent renormalization (SCR) model.[1,2] The SCR model was originally developed to account for weak itinerant-electron ferromagnets, where excellent quantitative agreement was observed.[1–4] In fact, the quantitative agreement achieved in these studies inspired the experimental search for ferromagnetic quantum criticality.[5]

However, all pure itinerant-electron ferromagnets studied experimentally so far show a first-order suppression of ferromagnetism when being tuned with a clean nonthermal control parameter, notably pressure.[6–9] Many different microscopic mechanisms exist, that may actually cause the first-order behavior observed. The most basic explanation is connected with maxima of the single-particle density of states in the vicinity of the Fermi level. Further, magnetoelastic coupling and weak spin-orbit interactions may also cause first-order behavior.[10–14] Theoretical studies have even established that pure many-body interactions may cause a first-order transition near ferromagnetic quantum criticality.[12] This suggests that ferromagnetic quantum criticality does not occur in pure materials.

Unlike the experimental and theoretical evidence that ferromagnetic quantum criticality does not exist in pure materials, ferromagnetic quantum criticality seems to occur under compositional tuning in systems such as $Pd_{1-x}Ni_x$ or $Nb_{1-y}Fe_{2+y}$.[15–17] This raises the question for the origin of quantum criticality in the presence of disorder. In particular, ferromagnetic quantum criticality has attracted great interest as a platform for so-called Griffiths phases and rare regions.[18]

The role of disorder and defects at a QPT alludes to weak-energy scales and how they affect the physical properties near QPTs as a more general theme. Since QPTs by construction may be reached when strong scales in the internal energy are balanced, one might naively expect that weak interactions can eventually stabilize novel behavior. A simple example is magnetically mediated superconductivity at a ferromagnetic QPT, where (weak) superconductive interactions dominate the ground state in a small parameter range.[19–23] Taking together the search for quantum criticality in itinerant-electron magnets and the question for the role of weak interactions make it of great interest to identify systems in which these issues may be studied in a controlled manner.

In this paper we address the question of quantum phase transitions in the transition-metal compounds $Mn_{1-x}Fe_xSi$ and $Mn_{1-x}Co_xSi$. These compounds are essentially ferromagnetic, where the ferromagnetism is subject to weak chiral spin-orbit couplings, also known as Dzyaloshinsky-Moriya (DM) interactions. Our investigation was inspired by extensive studies of the magnetic phase diagram and the pressure dependence of the itinerant helimagnet MnSi.

In the next section we present an extended introduction to the properties of MnSi in order to motivate the wide range of issues addressed in our study. This is followed by a more detailed account of the objectives and outline of the paper. In Sec. III we describe the single-crystal growth as well as the experimental methods. The presentation of the results is given in Secs. IV–VI for the magnetization, susceptibility,

and specific heat, respectively, followed by concluding remarks in Sec. VII.

II. EXTENDED INTRODUCTION

In MnSi rich phase diagrams that originate in a hierarchy of well-separated energy scales unfold in MnSi as a function of temperature, magnetic field, and pressure. On the strongest scale ferromagnetic exchange interactions favor parallel spin alignment. This is followed by spin-orbit interactions that are about one order of magnitude weaker. Due to the lack of inversion symmetry of the B20 crystal structure the spin-orbit interactions in leading order assume the rotationally invariant Dzyaloshinsky-Moriya form, i.e., they are proportional to $\mathbf{M}\cdot\nabla\times\mathbf{M}$, where $\mathbf{M}$ is the magnetization. Thus the spin-orbit interactions favor perpendicular spin alignment with a unique chirality. The combination of ferromagnetic exchange and DM interactions stabilizes long-wavelength helical spin order, where $\lambda_h \approx 180$ Å. The chirality of the helical modulation derives from the lack of inversion symmetry of the crystal structure and depends on the details of the electronic structure. The third and weakest scale in MnSi, which determines the direction of helical modulation, are higher order spin-orbit interaction terms, also referred to as crystal electric field interactions. In MnSi the helical modulation is pinned to the set of $\langle 111\rangle$ directions.

In the following we review the status of the experimental and theoretical understanding of MnSi. We begin with the ambient pressure properties, where we focus at first on the ferromagnetic limit, followed by the consequences of the DM interactions. We then turn to the experimental studies of the QPTs in MnSi under pressure. This sets the stage for an introduction of the properties of $Mn_{1-x}Fe_xSi$ and $Mn_{1-x}Co_xSi$ as reported in the literature prior to the work reported here.

A. Weak itinerant ferromagnetism in MnSi

In the 1970s and 80s the consequences of the hierarchy of energy scales in MnSi were addressed as separate issues. The first strand of developments concerned extensive studies of MnSi as a material close to itinerant-electron ferromagnetism, i.e., the helical modulation was considered to be a small distortion of an otherwise ferromagnetic state (the volume fraction of the Brillouin zone occupied by the helical modulation is only around 10^{-3}). The weak itinerant ferromagnets addressed in these studies are characterized by a strong Curie-Weiss dependence in the paramagnetic regime with a large fluctuating moment of order μ_B. The Curie-Weiss moment thereby exceeds the ordered magnetic moment, which is typically not larger than a few tenths of a μ_B (hence the name "weak" magnetism). Also unusual is the temperature dependence of the square of the ordered moment which varies as the square of the temperature $M_s^2(T)=M_0^2(1-T^2/T_c^2)$ where $M_0=M_s(T\rightarrow 0)$. Moreover, the magnetization is highly unsaturated and the nonlinear field dependence well described as $B/M\propto M^2$ (this is shown in so-called Arrott plots).

The properties of weak itinerant ferromagnets may be accounted for quantitatively in a phenomenological model taking into account the spectrum of thermal spin fluctuations.[1–3] Inelastic neutron scattering in MnSi established thereby for the first time in any material, the existence of the relevant thermal spin fluctuations over the entire Brillouin zone.[24,25]

For the discussion of the experimental results reported in this paper it is helpful to review the key expressions of the spin-fluctuation model of weak itinerant ferromagnets.[1] The model is based on a Ginzburg-Landau expansion of the free energy, where the magnetic field B that stabilizes the magnetization M is given by the usual magnetic equation of state

$$B(M)=\frac{1}{V}\frac{\partial F}{\partial M}=AM+bM^3. \tag{1}$$

The temperature-dependent inverse susceptibility

$$A=a+b[3\langle m_{\parallel}^2\rangle+2\langle m_{\perp}^2\rangle] \tag{2}$$

takes into account the effects of thermal spin fluctuations, where $\perp$ and $\parallel$ denote fluctuations transverse and longitudinal to the local magnetization, respectively. The effects of zero-point fluctuations are thereby included in the parameters a and b and only the effects of thermal contributions to the spin fluctuations are treated explicitly,[1] i.e., $\langle m^2\rangle\rightarrow 0$ for $T\rightarrow 0$. Note that the thermal fluctuations in general depend also on the magnetization M so that $A=A(M,T)$. The phenomenological parameters a and b represent the zero-temperature inverse initial susceptibility and the initial mode-mode coupling parameter. The zero-temperature ordered moment, $m_{s,0}$, is hence given by $-a/b=m_{s,0}^2$. In our study we exploit that a and b may be determined directly from the magnetic field dependence of the magnetization.

The variance of the spectrum of thermal spin fluctuations $\langle m_{\nu}^2\rangle$, where $\nu=\parallel$ or $\perp$, may be computed directly from the dynamical susceptibility $\chi(\mathbf{q},\omega)$ by means of the fluctuation-dissipation theorem

$$\langle m_{\nu}^2\rangle=4\hbar\int_{\text{first BZ}}\frac{d^3\mathbf{q}}{(2\pi)^3}\int_0^{\infty}\frac{d\omega}{2\pi}n(\omega)\text{Im }\chi_{\nu}(\mathbf{q},\omega), \tag{3}$$

where the $\mathbf{q}$ integral is over the first Brillouin zone. In the paramagnetic state the dynamical susceptibility is approximated by the double Lorentzian of an overdamped harmonic oscillator

$$\chi_{\nu}^{-1}(\mathbf{q},\omega)=\chi_{\nu}^{-1}(\mathbf{q})\left[1-\frac{i\omega}{\Gamma_{\nu}(\mathbf{q})}\right], \tag{4}$$

where the imaginary part of the dynamical susceptibility is given by

$$\text{Im }\chi_{\nu}(\mathbf{q},\omega)=\chi_{\nu}(\mathbf{q})\frac{\omega\Gamma_{\nu}(\mathbf{q})}{\omega^2+\Gamma_{\nu}^2(\mathbf{q})} \tag{5}$$

with

$$\chi_{\nu}^{-1}(\mathbf{q})=\chi_{\nu}^{-1}+c_{\nu}q^2+\cdots \tag{6}$$

and the relaxation frequency spectrum

$$\Gamma_{\nu}(\mathbf{q})=\gamma_{\nu}q\chi_{\nu}^{-1}(\mathbf{q}). \tag{7}$$

The spin-fluctuation spectrum is hence parametrized in terms of two phenomenological constants c_{ν} and γ_{ν}. Values of c

and γ in cgs and SI units differ by a factor 4π, i.e., $c_{\mathrm{cgs}}=4\pi c_{\mathrm{SI}}$ and $\gamma_{\mathrm{cgs}}=(4\pi)^{-1}\gamma_{\mathrm{SI}}$. In the ferromagnetic state as well as in the polarized state at finite magnetic field the fluctuation spectrum is more complex. In particular, one has to distinguish between a transverse part, that includes the usual spin-wave excitations and a longitudinal part. In addition the dynamics now also depends on the splitting of spin-up and spin-down Fermi surfaces.

The spin-fluctuation model of weak itinerant ferromagnetism described above accounts essentially for all of the experimental properties listed above. In particular, it relates the fluctuating Curie-Weiss moment to the small ordered moment and the nonlinear magnetization. Most impressively, perhaps, as first pointed out by Lonzarich[1,3] spin-fluctuation theory allows to calculate the ferromagnetic transition temperature T_c in quantitative agreement with experiment. Assuming that c and γ are isotropic T_c may be expressed in terms of the four phenomenological parameters a, b, c, and γ (in SI units) as follows:

$$T_c = 2.387c\left(\frac{-a}{b}\right)^{3/4}\frac{(\hbar\gamma)^{1/4}}{k_B}\mu_0^{3/4}. \tag{8}$$

The factor $\mu_0^{3/4}$ originates in the conversion from cgs to SI units. In our study of $Mn_{1-x}Fe_xSi$ and $Mn_{1-x}Co_xSi$ we consider the consistency with these expressions.

B. Helimagnetism in MnSi

The second strand of experimental studies in MnSi concerned the nature of the long-wavelength helimagnetic order. Already at the end of the 1950s Dzyaloshinsky[26] and Moriya[27] had shown that spin-orbit interactions may induce a canting of magnetic moments in antiferromagnets lacking inversion symmetry. In a pioneering effort Dzyaloshinsky showed theoretically that magnetic order may even get twisted into long-period helices in crystals lacking inversion symmetry, if the spin-orbit interactions are strong enough.[28]

To describe these magnetic modulations Dzyaloshinsky considered so-called Lifshitz invariants, i.e., certain antisymmetric terms in the Ginzburg-Landau free energy. These terms had been ruled out at first by the founding fathers of Landau theory as they destroy the homogeneity of condensed-matter systems. Since then many incommensurate ordered phases in crystalline materials have been discovered that may be described by Lifshitz invariants.[29] Thus inhomogeneities associated with Lifshitz invariants provide tremendously rich physical phenomena in a wide range of different systems, of which Dzyaloshinskys incommensurate magnetic helices are a simple example. The uniqueness of the chirality thereby distinguishes modulated magnetic states due to Dzyaloshinsky-Moriya interactions from spin spirals due to geometric frustration, e.g., in the magnetic rare-earth elements. Remarkably, it was only in the 1980s when the first experimental example of a Dzyaloshinsky-Moriya spiral was identified in a real material: the transition-metal compound MnSi.[30–34] The unique relationship between the chirality of the crystal lattice and the helimagnetic spin order was demonstrated a few years later.[35,36]

The magnetic phase diagram of MnSi is composed of five different phases. At high temperatures MnSi is paramagnetic, exhibiting a Curie-Weiss dependence with a large fluctuating moment, $m_{\mathrm{CW}}\approx 2.2\ \mu_{\mathrm{B}}$ f.u.$^{-1}$. Below $T_c=29.5$ K MnSi orders helimagnetically. The pitch of the helix is large, $\lambda_{\mathrm{h}}\approx 180$ Å, as compared to the lattice constant, $a=4.56$ Å. In an applied magnetic field the magnetic phase diagram is essentially isotropic, i.e., there are only small differences of the phase boundaries as a function of the direction of the applied magnetic field.

Well below T_c the application of a magnetic field causes a reorientation of the helical modulation for magnetic fields exceeding $B_{c1}\approx 0.1$ T.[31,37,38] For $B>B_{c1}$ the propagation direction of the helical modulation is thereby parallel to the applied magnetic field, i.e., the moments are perpendicular to the field as for spin-flop phases in antiferromagnets. For increasing field the moments become increasingly parallel to the applied field, thus forming a conical helix. Above $B_{c2}\approx 0.6$ T the helical modulation is suppressed and a weakly spin-polarized (ferromagnetic) state survives in high magnetic fields.

The Ginzburg-Landau treatment can be extended straightforwardly to helimagnets. For simplicity, we restrict the following discussion to isotropic helimagnets. This includes the Dzyaloshinsky-Moriya interaction and properly captures the transition at B_{c2}. For a description of the reorientation transition at B_{c1} crystal anisotropies must be included in the theory. The Ginzburg-Landau potential of the magnetization $\mathbf{M}$ for an isotropic helimagnet reads

$$\mathcal{V}(\mathbf{M}) = \frac{a}{2}\mathbf{M}^2 + \frac{b}{4}(\mathbf{M}^2)^2 + \frac{D}{2}\mathbf{M}(\nabla\times\mathbf{M}) - \frac{c}{2}\mathbf{M}\nabla^2\mathbf{M} - \mathbf{B}\mathbf{M} \tag{9}$$

with the Dzyaloshinsky-Moriya interaction amplitude D. In an extended regime of the phase diagram (except the A phase) the potential can be minimized with the help of the conical-helix Ansatz for the magnetization as a function of position $\mathbf{r}$

$$\mathbf{M}(\mathbf{r}) = M\hat{\mathbf{B}} + M_Q\cos(\mathbf{Q}\mathbf{r})\hat{\mathbf{e}}_1 + M_Q\sin(\mathbf{Q}\mathbf{r})\hat{\mathbf{e}}_2, \tag{10}$$

where $\mathbf{Q}$ is the pitch vector of the helix that is oriented in the direction of the magnetic field, $\mathbf{Q}=Q\hat{\mathbf{B}}$. The unit vectors $\hat{\mathbf{e}}_1$ and $\hat{\mathbf{e}}_2$ obey

$$\hat{\mathbf{e}}_1\times\hat{\mathbf{e}}_2 = \hat{\mathbf{Q}}. \tag{11}$$

The Ginzburg-Landau potential Eq. (9) then simplifies to a function of three parameters

$$\mathcal{V}(M,M_Q,Q) = \frac{a}{2}(M^2+M_Q^2) + \frac{b}{4}(M^2+M_Q^2)^2 - \frac{D}{2}M_Q^2Q + \frac{c}{2}M_Q^2Q^2 - MB. \tag{12}$$

Minimization leads to the three equations

$$\frac{\partial\mathcal{V}}{\partial M} = aM + b(M^2+M_Q^2)M - B = 0, \tag{13}$$

$$\frac{\partial \mathcal{V}}{\partial M_Q} = aM_Q + b(M^2 + M_Q^2)M_Q - DQM_Q + cQ^2M_Q = 0, \tag{14}$$

$$\frac{\partial \mathcal{V}}{\partial Q} = -\frac{D}{2}M_Q^2 + cM_Q^2Q = 0. \tag{15}$$

In the presence of a finite $M_Q > 0$, it is possible to solve Eq. (15) for the pitch of the magnetic helix

$$Q = \frac{D}{2c}, \tag{16}$$

which is proportional to the Dzyaloshinsky-Moriya interaction D. With this solution Eq. (14) simplifies to

$$a + b(M^2 + M_Q^2) - \frac{D^2}{4c} = 0. \tag{17}$$

Assuming that this equation has a solution we may simplify Eq. (13) as follows:

$$\frac{B}{M} = \frac{D^2}{4c} = cQ^2. \tag{18}$$

In the conical phase the magnetization increases linearly with the field B, and the slope is given by the square of the pitch vector Q. Inserting Eq. (18) in Eq. (17) we finally obtain for M_Q

$$M_Q = \frac{1}{\sqrt{b}}\sqrt{cQ^2 - a - b\left(\frac{B}{cQ^2}\right)^2} \tag{19}$$

provided that the magnetic field is sufficiently small

$$|B| < B_{c2} = cQ^2\sqrt{\frac{cQ^2 - a}{b}} \tag{20}$$

and $a < cQ^2$. This determines the upper critical field B_{c2} below which the conical helix is stabilized. For higher fields $B > B_{c2}$ one enters the homogeneously polarized state $M_Q = 0$. In this regime the minimization conditions in Eqs. (13)–(15) reduce to the equation of state [Eq. (1)] of the ferromagnet.

Similar as for the ferromagnet, see Eq. (2), the helimagnetic fluctuations renormalize the Ginzburg-Landau potential Eq. (9) and, in particular, lead to a temperature dependence of the parameter $a \to A$ that controls the distance to the transition. For energies larger than the spin-orbit gap of the Fermi surface and momenta larger than the Dzyaloshinsky-Moriya interaction D, these fluctuations have an essentially ferromagnetic character. In the limit of small energies and momenta, however, the fluctuation spectrum will differ from that of an itinerant ferromagnet and the renormalizations will reflect the particular properties of metals with spin-orbit coupling.[39] In order to analyze the dependence of the magnetization on magnetic field, we approximate the equation of state for fields $B > B_{c2}$ close to B_{c2} as

$$\frac{B}{M} \approx A(M_{c2}, T) + bM^2 \tag{21}$$

with $B_{c2} = cQ^2M_{c2}$ so that the Arrott plot B/M vs M^2 is approximated to be linear. Using Eq. (21), we experimentally extract the parameters $A(M_{c2}, T)$ and b and discuss their dependences on temperature and doping.

C. Skyrmion lattice in MnSi

For temperatures just below T_c a small phase pocket, referred to as the A phase,[37] was first observed in ultrasound attenuation and magnetization studies. As a function of magnetic field the A phase is bounded by the transition fields $B_{A1} < B_{A2}$. The A phase was initially interpreted as a paramagnetic state. However, neutron scattering already in the early 1990s established the existence of a helical modulation *perpendicular* to the applied field, where just a single modulation vector had been observed.[40,41] In comparison to spin-flop phases of normal antiferromagnets a single helical modulation perpendicular to the applied field is energetically highly unfavorable and there was no satisfactory theoretical account for a long time.[42,43]

In fact, recently we managed to show that the early work on the A phase in MnSi was incomplete. Originally inspired by our high-pressure studies of the QPTs in pure MnSi (Ref. 44) and the search for spin-transfer torque effects at ambient pressure[45] we revisited the magnetic structure in the A phase. Small angle neutron scattering (SANS) revealed a sixfold scattering pattern when the incident neutron beam is parallel to the applied magnetic field.[46] This implied at least a multi-**k** structure, which, however, turned out to be a new form of magnetic order: a skyrmion lattice.

As its most remarkable feature the spin structure in the A phase supports a nontrivial topology, notably the winding number of the magnetic unit cell is −1. The evidence for the skyrmion lattice was initially based on the excellent theoretical account of all properties observed experimentally. According to the theoretical model proposed in Ref. 46 the A phase is thereby stabilized by thermal Gaussian fluctuations. The observation of a topological Hall signal proved the existence of the topological properties beyond doubt.[47] Thus the spin structure in the A phase corresponds to a hexagonal lattice of antiskyrmions, which may be pictured as a hexagonal lattice of a kind of spin vortices parallel to the applied field. By now the same type of magnetic order has also been observed in the A phase of the doped semiconductor $Fe_{1-x}Co_xSi$ (Ref. 48) and the single crystals of $Mn_{1-x}Fe_xSi$ and $Mn_{1-x}Co_xSi$ studied in this paper (a preliminary report on the observed skyrmion lattices has been published in Ref. 49). In fact, recently individual skyrmions have been observed by means of Lorentz force microscopy in $Fe_{1-x}Co_xSi$ ($x=0.5$).[50,51]

D. Magnetic quantum phase transition in MnSi

The self-consistent RPA of itinerant-electron ferromagnetism is deeply rooted in Landau-Fermi-liquid theory. However, since the early days of the RPA it was appreciated that a phase transition to itinerant-electron ferromagnetism pre-

cisely at $T=0$ would imply an inconsistency with the starting assumption of Fermi-liquid theory.[52,53] The fermion quasiparticle interactions were thereby expected to become singular resulting in a *marginal* breakdown of Fermi-liquid theory. This motivated theoretical and experimental studies of zero-temperature magnetic to nonmagnetic phase transitions.[5,54,55] These first efforts have developed into the field of quantum phase transitions, defined as phase transitions driven by quantum fluctuations.

The controlled search for a marginal breakdown of Fermi-liquid theory in itinerant-electron magnets began with studies of MnSi, where hydrostatic pressure was used as a clean tuning parameter.[5,56] While the resistivity suggested a continuous suppression of the magnetic order at a pressure $p_c = 14.6$ kbar measurements of the ac susceptibility established soon that the associated QPT is actually first order.[57] As the perhaps most puzzling property, it was further found that the temperature dependence of the electrical resistivity abruptly changes at the critical pressure from the quadratic dependence of a Fermi liquid to an extended, stable $T^{3/2}$ non-Fermi-liquid NFL form.[58]

To explore the origin of the non-Fermi-liquid resistivity neutron-scattering studies of the helical order were carried out, revealing that the ordered moment is not suppressed at p_c.[44] Instead, considerable scattering intensity was found to survive above p_c. However, in contrast to ambient pressure the scattering intensity above p_c is distributed everywhere over the surface of a small sphere in reciprocal space with broad intensity maxima for the crystallographic $\langle 110 \rangle$ directions. As the magnetic scattering intensity qualitatively shares similarity with the structural scattering intensity observed in liquid crystals, the magnetic state above p_c is referred to as partial magnetic order.

The intensity maxima in the partially ordered state for $\langle 110 \rangle$ and their temperature dependence as compared with the normal helical order early on suggested phase separation and that the partial order is not just composed of disordered helices. This was, in particular, supported by the magnetic field dependence observed in small angle neutron scattering.[59] In addition the small angle neutron scattering established that B_{c1} and B_{c2} are essentially unchanged as a function of pressure and the ordered moment in a small applied field extrapolates to zero around 40–50 kbar (see also Ref. 60).

In turn the observation of the partial magnetic order inspired various proposals of chiral spin textures with nontrivial topology such as merons and skyrmions as the dominant property of the high pressure state.[61–65] To obtain thermodynamic information on the QPT in MnSi high-resolution measurements of the lattice constants as a function of pressure using Larmor diffraction were carried out.[66] These data established beyond doubt, that there is no quantum critical point (QCP) under pressure in MnSi (we use the expression QCP exclusively for second-order quantum phase transition). The same data also show the formation of phase separation in the range $p^* < p < p_c$. The magnetoelastic contribution as extrapolated to zero temperature thereby tracks the helimagnetic volume fraction inferred from the μSR study.[67,68] The absence of quantum criticality is inferred from the change from magnetoexpansion to magnetostriction at p_c, which takes place around $T \approx 12$ K. The Larmor data thereby show that the regime of the non-Fermi-liquid resistivity is accompanied by a magnetostriction at 20 kbar of roughly $a_2 \approx 4 \times 10^{-5}$. The same magnetostriction may be also inferred from forced magnetostriction measurements reported by Miyake *et al.*[49,69] This suggests that the non-Fermi-liquid resistivity is an intrinsic property of a novel metallic regime that emerges under pressure.

E. Introduction to $Mn_{1-x}Fe_xSi$ and $Mn_{1-x}Co_xSi$

For a long time it has been known that substitutional replacement of Mn with Fe or Co suppresses the helimagnetic order in MnSi. This offers a different route to obtain a magnetic quantum phase transition. First magnetization and NMR studies[70] in $Mn_{1-x}Co_xSi$ showed that the magnetization curves are qualitatively unchanged under Co doping and suggested a critical concentration in polycrystalline samples of $x_c^{Co} \approx 0.08$. This was followed by small angle neutron scattering, resistivity, and magnetization measurements in $Mn_{1-x}Co_xSi$, which established that the helimagnetic wavelength decreases by a factor of two under Co doping.[71] These studies also showed a metallic state and an increasing residual resistivity characteristic of increased defect scattering. A more comprehensive study of the magnetic order in various B20 compounds including selected compositions of $Mn_{1-x}Fe_xSi$ and $Mn_{1-x}Co_xSi$ established helimagnetic spin spirals as a rather general property in these systems.[72] At the same time $Mn_{1-x}Fe_xSi$ studies for large values of x showed that Mn may be used to suppress the excitation gap in the insulator FeSi.[73]

In recent years a number of experimental studies focused on the magnetotransport properties of $Mn_{1-x}Fe_xSi$ and $Mn_{1-x}Co_xSi$. These studies were partly inspired by the search for unconventional metallic properties and anomalies of the Hall effect.[74–76] Quite recently small angle neutron scattering established that the magnetic phase diagram of $Mn_{1-x}Fe_xSi$ for $x=0.06$, 0.08, and 0.10 qualitatively does not change under doping.[77] In this study it was also concluded that the long-range order vanishes under Fe doping for $x > 0.13$, but the detailed suppression of the ordered moment was not reported. Moreover, it has been pointed out that the samples of $Mn_{1-x}Fe_xSi$ may be grown with both chiralities[78] as may be expected of all B20 compounds.

Recent studies of the temperature dependence of the electrical resistivity revisited the question of a quantum phase transition in $Mn_{1-x}Fe_xSi$. Even though non-Fermi-liquid behavior was observed at the critical concentration of $Mn_{1-x}Fe_xSi$ no detailed discussion of the possible nature of the NFL behavior was given.[79] As reported before, the residual resistivity was found to increase dramatically when approaching the critical concentration. Hence the nature of the possible quantum phase transition and the possible role of chiral spin interactions were an open issue prior to our study.

F. Objectives and outline

The high-pressure studies of MnSi raise the question for the nature of the partial magnetic order and its possible rela-

tionship to the non-Fermi-liquid resistivity. The recent identification of the A phase in MnSi as a skyrmion lattice establishes the existence of such spin textures with nontrivial topology. Thus a natural question concerns the fate of these spin textures when MnSi is tuned to a QPT. However, since high hydrostatic pressures are extremely challenging experimentally it is also interesting to consider alternative tuning techniques to achieve a QPT.

This raises the question for thermodynamic evidence of the QPTs in $Mn_{1-x}Fe_xSi$ and $Mn_{1-x}Co_xSi$ and whether there exists a quantum critical point (unlike for pressure tuning). Moreover, how does the hierarchy of energy scales evolve under doping and what is the fate of the various magnetic phases? In particular, how do the QPTs in $Mn_{1-x}Fe_xSi$ and $Mn_{1-x}Co_xSi$ compare with pure MnSi under pressure? Here an important issue concerns the role of disorder and whether the disorder stabilizes the existence of quantum criticality.

In this paper we report a comprehensive study of the magnetization, ac susceptibility and specific heat of optically float-zoned single crystals of $Mn_{1-x}Fe_xSi$ and $Mn_{1-x}Co_xSi$. The magnetization data as recorded for magnetic fields that are sufficient to suppress the helical modulations point to an underlying ferromagnetic quantum critical point in both $Mn_{1-x}Fe_xSi$ and $Mn_{1-x}Co_xSi$. The ac susceptibility and specific heat consistently suggest an important role of the Dzyaloshinsky-Moriya interactions in the noncentrosymmetric crystal structure near this underlying ferromagnetic quantum critical point. With increasing concentration a QPT is related to the suppression of long-range helical order; a second important scale is related to the suppression of a Vollhardt invariance[80,81] in the specific heat at the onset of an intermediate regime between paramagnetism and helical order.

We have also performed comprehensive small angle neutron scattering studies and magnetotransport measurements.[82,83] These studies will be reported elsewhere. As the main result of our SANS studies we find that the suppression of helimagnetic order in both $Mn_{1-x}Fe_xSi$ and $Mn_{1-x}Co_xSi$ is accompanied by an increase in the magnetic mosaicity transverse to the ordering vector. This may be due to the weak disorder. The neutron-scattering studies further confirm the magnetic phase diagrams inferred from the magnetization and susceptibility. In particular, the skyrmion lattice structure in the A phase is insensitive to the disorder and defects introduced by doping. Our magnetotransport studies thereby confirm the existence of the nontrivial topology of the spin structures. Inelastic neutron-scattering studies are currently under way.

The presentation of the work reported in this paper proceeds as follows. In Sec. III we describe the experimental methods, notably the preparation of the single crystals using optical float zoning and aspects of the specific heat and magnetization measurements. This is followed by sections on the magnetization (Sec. IV), ac susceptibility (Sec. V), and specific heat (Sec. VI), each composed of a section presenting the experimental results followed by a discussion. Given the mere volume of data the immediate discussion of the experimental results allows us to bring out better the salient features of our study. The paper concludes with a discussion of the results in Sec. VII.

III. EXPERIMENTAL METHODS

The preparation of the single-crystal samples of $Mn_{1-x}Fe_xSi$ and $Mn_{1-x}Co_xSi$ involved three steps: (i) the purification of the starting elements, (ii) the preparation of polycrystalline rods, and (iii) single-crystal growth by optical float zoning. For the growth of the single-crystal samples we used 4N Mn, 4N Fe, 3N5 Co, and 6N Si. The Mn and Fe were first carefully etched followed by a thorough ultrasonic cleaning. Using a bespoke Huykin crucible with radio-frequency heating inside an all-metal sealed furnace we cast rods of pure Mn and Fe under purified 6N Ar gas.

The same rod-casting furnace was also used to prepare polycrystalline rods of $Mn_{1-x}Fe_xSi$ and $Mn_{1-x}Co_xSi$ for the optical float zoning. From the high-purity rods of Mn and Fe and the Co and Si the starting weight of the ingots was prepared with an accuracy around ± 1 mg. The Fe and Co pieces were thereby etched to weight. The typical weight of the ingots was ~ 12 g. The starting elements were molten several times, where the polycrystalline pellets were flipped over each time after melting to ensure maximum homogeneity. In a final step the polycrystalline pellets were cast into rods with a diameter of $d=6$ mm and a length between $l \approx 30$ and 60 mm.

The single crystals of $Mn_{1-x}Fe_xSi$ and $Mn_{1-x}Co_xSi$ were grown in a four-mirror image furnace (Crystal Systems Incorporation). To provide ultrahigh vacuum compatible conditions our furnace was refurbished to be all-metal sealed.[84] After mounting the polycrystalline starting rods the furnace was thoroughly pumped-down using a turbo pump, baked out using bespoke heating jackets and filled with a 6N Ar atmosphere that had been purified additionally by means of a hot getter furnace (NuPure).

For the optical float zoning two polycrystalline rods were mounted in the image furnace. The samples were first float zoned to a starting position close to the lower end of the polycrystalline rods. At the beginning of the final float-zoning passage we applied a necking of the zone to promote single-crystal grain selection, followed by float zoning over the entire distance with a speed $v_{fz} \approx 5$ mm h^{-1}. During the float zoning the feed and seed rods were counter-rotating with $f_{fz} \approx 10$ min^{-1}.

The float-zoned rods were first characterized by Laue x-ray diffraction along the entire length to identify large single-crystal grains. In addition selected sections (notably the final zone) were cut, polished mechanically and checked with an optical microscope. For all compositions the final zone exhibited a convex interface with respect to the polycrystalline feed rod. In all samples grown we observed a very stable growth process. We have confirmed in several ingots that the physical properties of samples from the start and the end of the float-zoned ingots were identical. This provided evidence for an excellent homogeneity of the composition along the samples (Fig. 1).

Shown in Table I is a summary of all crystals grown and the size of the single-crystal grains they contained. For the various measurements single-crystal specimens were cut from the ingots using a diamond wire saw. The samples were oriented by means of x-ray Laue diffraction. For the bulk measurements a ⟨110⟩-oriented disc was prepared (thickness

FIG. 1. (Color online) Single crystals of MnSi, $Mn_{1-x}Fe_xSi$, and $Mn_{1-x}Co_xSi$ grown for our study. For each panel the growth direction was from the right to the left. In most crystals a necking was applied at the beginning of the growth to promote grain selection.

1 mm) from which samples were cut according to the same layout shown in Fig. 2. The notation is as follows: (a) parallelepiped $1\times1\times6$ mm^3 for magnetization and ac susceptibility with $B\|\langle100\rangle$; (b) quarter of a cylindrical disc perpendicular to $\langle110\rangle$ with a radius of 3 mm and thickness of 1 mm for specific-heat measurements; (c) and (d) thin platelets $0.2\times1\times6$ mm^3 and $0.2\times1\times3$ mm^3, respectively, for electrical transport, where current is parallel to $\langle100\rangle$ and field parallel to $\langle110\rangle$; (e) and (f) thin platelets $0.2\times1\times3$ mm^3 for electrical transport, where current is parallel to $\langle110\rangle$ and field parallel to $\langle100\rangle$; (g) cube $1\times1\times1$ mm^3 for measurements of orientational dependences. Using the same sample shape for the same measurements and different compositions allowed us to avoid systematic errors when comparing data.

The magnetization, ac susceptibility, and specific heat were measured with a Quantum Design Physical Properties Measurement System at temperatures down to ~2 K and in magnetic fields up to 9 T. The magnetization was thereby determined with an extraction technique. The specific heat was measured with a standard heat-pulse method, where typical heat pulses were around 1–2 %.

TABLE I. Summary of the single crystals grown for this study. Also shown are the extent of the necking and the size of the single-crystalline sections.

Composition		Single crystal	Necking
$Mn_{1-x}Fe_xSi$	x=0	20 mm	Strong
	x=0	40 mm	Strong
	x=0.04	40 mm	Strong
	x=0.08	4 mm (top)	None
	x=0.08	15 mm (top)	None
	x=0.12	2 grains	None
	x=0.12	40 mm	Weak
	x=0.16	60 mm	Strong
	x=0.19	30 mm	Strong
$Mn_{1-x}Co_xSi$	x=0.02	20 mm	Intermediate
	x=0.04	4 mm (top)	Weak
	x=0.04	25 mm	Strong

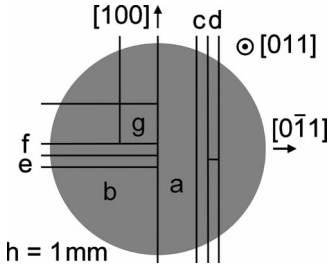

FIG. 2. Depiction how the $\langle110\rangle$-oriented disc was cut up (a $\langle110\rangle$ direction was parallel to the line of sight). This way samples for the various bulk properties measured in our study all had the same dimensions. See text for details of layout.

In all measurements the same systematic procedure was applied. Data as a function of temperature were always recorded for increasing temperature. We thereby carefully distinguished, whether the sample was initially zero-field cooled (zfc) or field cooled (fc) at the field value for which data were recorded. We also tested the role of high-field cooling (hfc), where the sample was cooled down in a field larger than the upper critical field B_{c2}. In magnetic field sweeps the sample was initially zfc to the temperature at which data were collected followed by a standard five-point loop.

The study we present in this paper focused on the crystallographic $\langle100\rangle$ direction. We have also measured other crystallographic directions for selected compositions. Typical data are described in the text, though we have no comprehensive account of the orientational dependence. However, these data are sufficient to conclude that B_{c2} is unchanged as a function of orientation, while there may be small changes in the precise location of B_{c1}, B_{A1}, and B_{A2}.

IV. MAGNETIZATION

In this section we present the magnetization of $Mn_{1-x}Fe_xSi$ and $Mn_{1-x}Co_xSi$. Following a first account of the results, we focus on the behavior in magnetic fields that are sufficiently strong to suppress the effects of the DM interactions, i.e., $B\geq B_{c2}$. From the field-induced ferromagnetic behavior we extrapolate the properties in zero magnetic field. In particular, we compare the ferromagnetic properties with the spin-fluctuation model of itinerant-electron ferromagnets given above. As our main conclusion the magnetic field dependence of the magnetization in both $Mn_{1-x}Fe_xSi$ and $Mn_{1-x}Co_xSi$ for the parameter range studied are consistent with an underlying ferromagnetic quantum critical point. The ac susceptibility and specific heat presented below suggest that this extrapolated ferromagnetic quantum critical point may be masked at low fields by a quantum phase transition due to helimagnetic order.

A. Experimental results of the magnetization

Shown in Fig. 3 is the magnetization at 4 K up to 9 T for various concentrations x. With increasing concentration the zero-field extrapolated ordered moment is suppressed while the increase in the magnetization at high fields, i.e., the high-

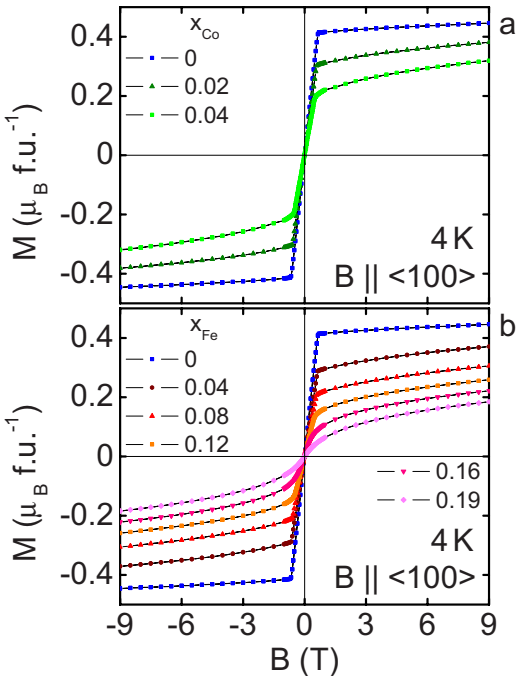

FIG. 3. (Color online) Isothermal magnetization of $Mn_{1-x}Co_xSi$ and $Mn_{1-x}Fe_xSi$ at 4 K as a function of field up to 9 T for various concentrations.

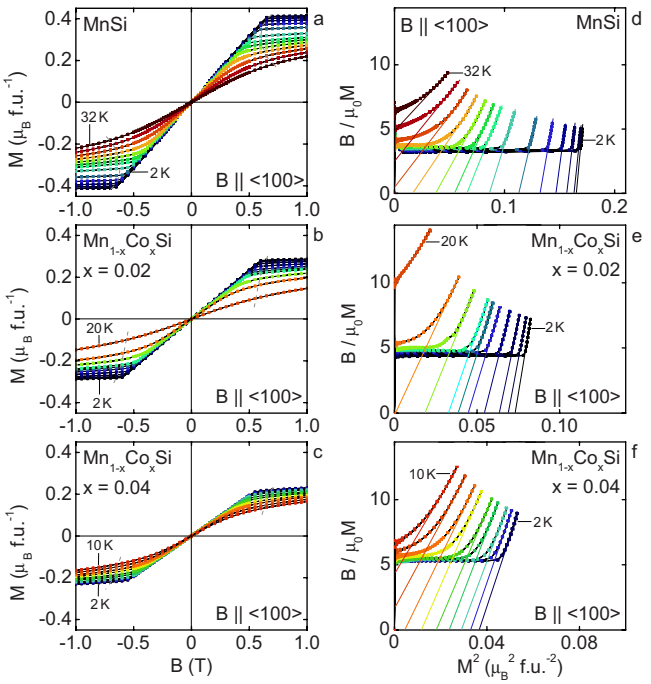

FIG. 4. (Color online) Typical magnetic field dependence of the magnetization of MnSi and $Mn_{1-x}Co_xSi$ for $x=0.02$ and 0.04. The magnetic field was parallel ⟨100⟩. The same qualitative behavior is observed in all compounds studied. For clarity only data in the field range ± 1 T are shown. Data were recorded up to 9 T at selected temperatures, where an unsaturated magnetization is observed down to the lowest temperatures studied.

field susceptibility, remains unchanged. For detailed information data were also recorded in magnetic fields up to 1 T for a large number of temperatures. Shown in Fig. 4 are typical data recorded for pure MnSi and $Mn_{1-x}Co_xSi$. The related magnetization of $Mn_{1-x}Fe_xSi$ is presented in Fig. 5.

For all samples studied the magnetic field dependence of the magnetization is nearly linear at high temperatures. With decreasing temperature, the magnetic field dependence of the magnetization becomes strongly nonlinear in the vicinity of T_c. At 2 K, the lowest temperatures studied, we observed a clear kink at the upper critical field B_{c2}. For fields $B<B_{c2}$ the magnetization is dominated by an increase that is essentially linear as expected from Eq. (18), followed by a very weak magnetic field dependence for $B>B_{c2}$. Even for the lowest temperatures investigated the magnetization of all samples studied is clearly unsaturated up to the highest fields measured (cf. Fig. 3). For all samples studied the behavior is consistent with pure MnSi as reported in the literature.[85,86]

For sufficiently large magnetic fields the magnetization in $Mn_{1-x}Fe_xSi$ and $Mn_{1-x}Co_xSi$ may be described rather well with a cubic magnetic equation of state ($B/M \propto M^2$). In comparison to $Mn_{1-x}Fe_xSi$ and $Mn_{1-x}Co_xSi$, the nonlinear magnetization of pure MnSi clearly deviates from a cubic magnetic equation of state. This has been known for quite sometime. A recent controversy in the literature[87–89] therefore seems somewhat surprising. Clearly, the precise description in the standard Ginzburg Landau scenario must be incomplete for pure MnSi.

To obtain the inverse linear susceptibility A and the lowest order mode-mode coupling parameter b from the magnetization, we have plotted B/M versus M^2 as shown in Figs. 4 and 5. The experimental data were only fitted for sufficiently high magnetic fields, where the helical modulation is suppressed and a linear relationship $B/M \propto M^2$ is observed, cf. Eq. (21). We find that the data deviate from such a proportionality for fields less than a few tenths of a tesla. Using the data at sufficiently high fields we inferred an ordered magnetic moment m_s as a function of temperature from the intercept of a linear extrapolation through the x axis, i.e., the value of M^2 for $B/M \to 0$.

The temperature dependence of the extrapolated value of m_s is shown in Fig. 6(a). With increasing temperature the ordered moment decreases monotonically and vanishes continuously at the transition temperature T_c. In other words, when suppressing the effects of the helical modulation in a small magnetic field the extrapolated ferromagnetic moment shows a second-order phase transition for all x studied. As described below the transition temperature T_c defined this way resides between two transition temperatures T_1 and T_2 inferred from the ac susceptibility and the specific heat, which reflect the DM interactions.

We find it remarkable that the temperature dependence of m_s is well described as $m_s^2=m_{s,0}^2(1-T^2/T_c^2)$ for all doped samples we studied as shown in Fig. 6(b). As mentioned in the introduction this is the typical behavior observed in weak itinerant ferromagnets (see, e.g., Ref. 6). In contrast, as shown in the inset of Fig. 6(b) the temperature dependence of m_s in pure MnSi inferred from $M(B)$ does not follow this temperature dependence. This is also denoted by the dashed line in Fig. 6(a).

With increasing concentration x the extrapolated transition temperature T_c, inferred from the onset of m_s, decreases

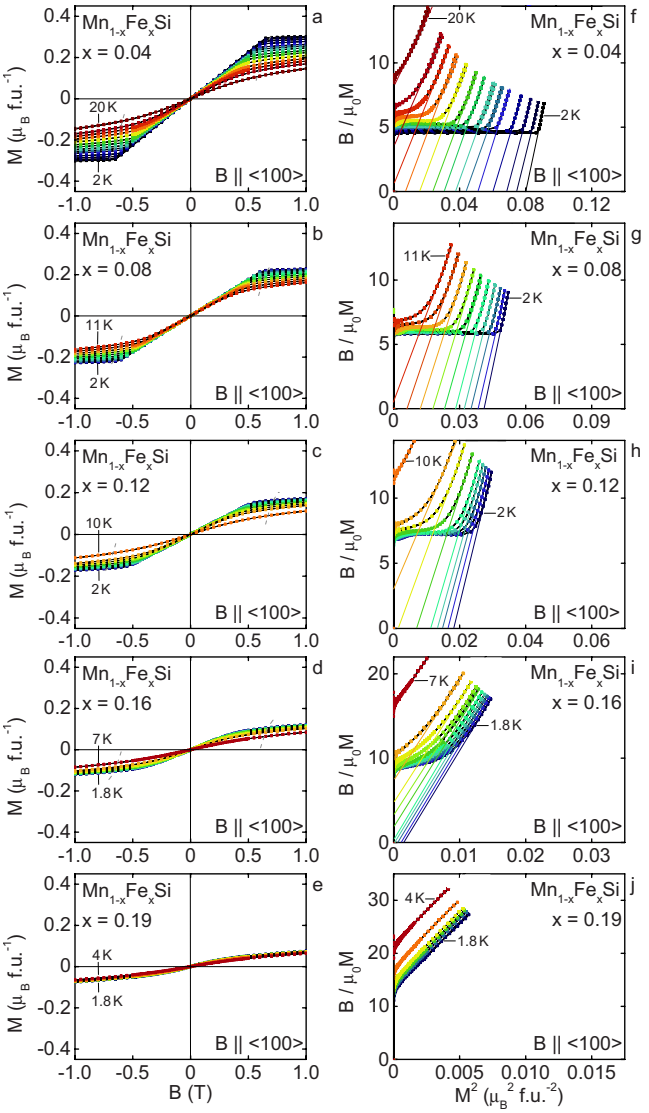

FIG. 5. (Color online) Typical magnetic field dependence of the magnetization of $Mn_{1-x}Fe_xSi$ for $x=0.04$, 0.08, 0.12, 0.16, and 0.19. The magnetic field was parallel ⟨100⟩. The same qualitative behavior is observed in all compounds studied. For clarity only data in the field range ±1 T are shown. Data were recorded up to 9 T at selected temperatures. The magnetization at high fields is unsaturated down to the lowest temperatures studied.

sublinear as shown in Fig. 7(a). This strongly contrasts typical pressure dependences of magnetic transition temperatures, which tend to be superlinear. In fact, the variation in T_c with x even raises the question, if T_c is suppressed altogether. However, we find purely empirically that the suppression of T_c is best accounted for by a square-root dependence, $T_c = T_c(x=0)(1-\sqrt{x/x_c})$ [Fig. 7(b)]. The rather unusual concentration dependence of T_c suggests consistently the existence of a critical concentration under Co and Fe doping of $x_c^{Co} \approx 0.084$ and $x_c^{Fe} \approx 0.192$, respectively. It is interesting to note that the critical concentrations differ by a factor of two, consistent with the different numbers of valence electrons of Fe and Co as compared to Mn.

As a function of increasing concentration x the extrapolated ordered moment m_s also decreases monotonically as

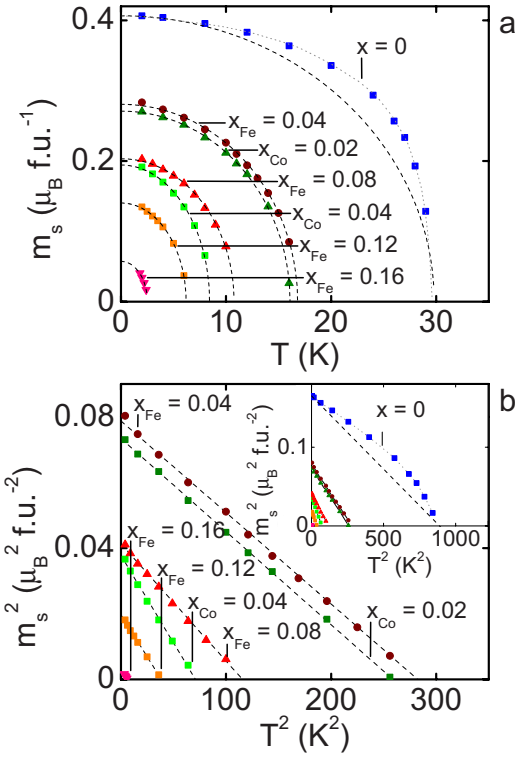

FIG. 6. (Color online) (a) Temperature dependence of the magnetic moment m_s of MnSi, $Mn_{1-x}Co_xSi$, and $Mn_{1-x}Fe_xSi$ as extrapolated from the ferromagnetically polarized regime. For all values of x we find a continuous temperature dependence, characteristic of critical transitions. (b) Square of the magnetic moment m_s^2 versus temperature squared T^2. The linear dependence observed for all x except pure MnSi is a key characteristic of itinerant ferromagnets.

shown in Fig. 8. The critical concentrations x_c inferred from $m_s \to 0$, $x_c^{Fe} \approx 0.19$ and $x_c^{Co} \approx 0.09$, are perfectly consistent with the critical concentrations determined from the magnetic ordering temperature. Shown in Fig. 8 is the suppression of m_s as a function of normalized concentration, showing the qualitative similarity of the effects of Fe and Co doping. In order to test whether the Fe and Co atoms support any magnetic polarization at all (FeSi and CoSi do not order magnetically), we additionally distinguish in Fig. 8 the ordered moment per formula unit as compared with the ordered moment per Mn atom. However, as the differences are small it is not possible to reach any conclusion on this issue. We also note that the critical concentrations under Fe and Co doping observed in our study are consistent with those reported in Refs. 70 and 75 while they differ from Ref. 77.

Since the variation in T_c and m_s with x seem highly unusual it is instructive to check for consistency with the general predictions of spin-fluctuation theory [cf. Eq. (8)], notably the relationship of the zero-temperature ordered moment $m_s(T \to 0) = m_{s,0}$ versus T_c. For the observed dependence $m_s^2 = m_{s,0}^2(1-T^2/T_c^2)$ (Fig. 6) one might expect $T_c \propto m_{s,0}$. Plotting T_c versus $m_s^{3/2}$ we find instead that $T_c \propto m_s^{3/2}$ over a remarkably wide range as suggested by Eq. (8) and shown in Fig. 9. To resolve this seeming contradiction between Figs. 6(b) and 9 we expect that careful consideration of transverse and longitudinal components of the spin-fluctuation spectra will be

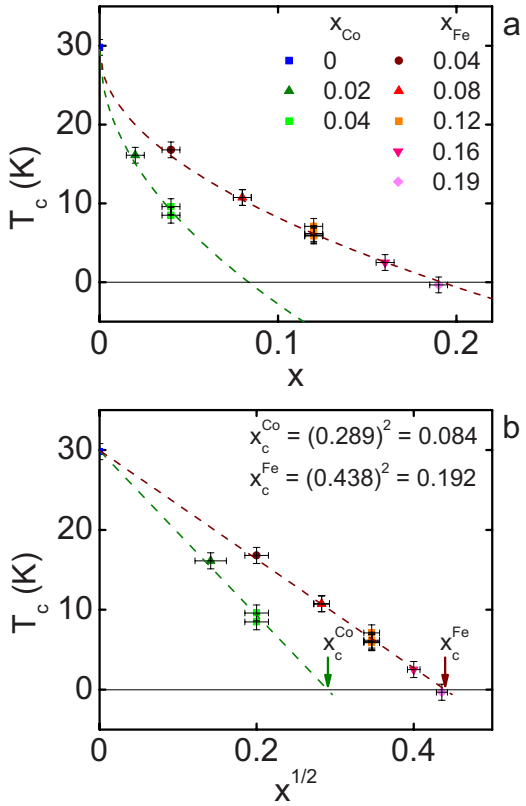

FIG. 7. (Color online) (a) Transition temperature as a function of concentration. A sublinear dependence is observed for both $Mn_{1-x}Fe_xSi$ and $Mn_{1-x}Co_xSi$. (b) Empirically the suppression is well accounted by a square-root dependence with the concentration. Note the values for the extrapolated critical concentrations given in the figure.

necessary. For comparison we also show in Fig. 9 the relationship of T_c versus $m_s^{3/2}$ of pure MnSi under pressure (here T_c was taken from Ref. 57 and m_s from Refs. 90 and 91; see also Ref. 59). It is thereby interesting to note that the point of inflection of the data shown in Fig. 9 coincides with the tricritical point at $p^* \approx 12$ kbar and $T^* \approx 12$ K inferred from the onset of itinerant metamagnetism.[57,92]

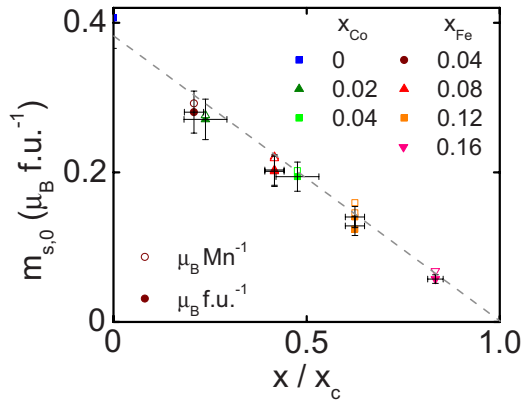

FIG. 8. (Color online) Suppression of m_s inferred from the field dependence of the magnetization in the ferromagnetic regime on a normalized concentration scale.

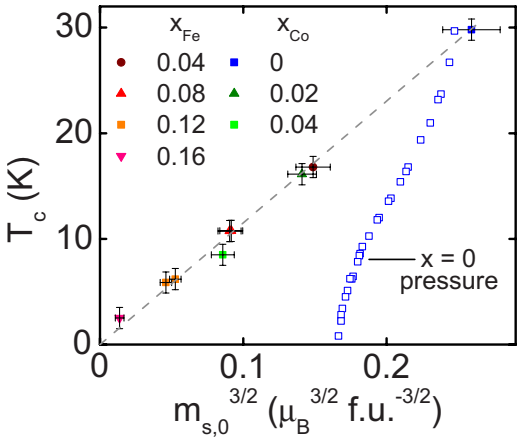

FIG. 9. (Color online) Transition temperature T_c versus ordered magnetic moment $m_s^{3/2}$, both inferred from Arrott plots of the magnetization. The proportionality observed here extents over a remarkably wide range and strongly suggests the existence of an underlying ferromagnetic quantum critical point. The data points labelled "x=0 pressure" have been inferred from Refs. 57, 90, and 91.

We note that both the transition temperature and the ordered moment vary by over 80% in our doping studies. The relationship $T_c \propto m_s^{3/2}$ hence covers a remarkably wide range and seems not just fortuitous. In contrasts, as a function of pressure the ordered moment m_s in MnSi vary by several ten percent up to the critical pressure p_c, where T_c vanishes. Keeping in mind that the quantities we discuss here have been inferred from the ferromagnetic regime of the Arrott plots, the relationship we observe experimentally suggests strongly, that the ferromagnetic exchange, representing the strongest energy scale in both $Mn_{1-x}Co_xSi$ and $Mn_{1-x}Fe_xSi$, leads to an underlying ferromagnetic quantum critical point. In turn this raises the question for modifications of ferromagnetic quantum criticality due to the much weaker energy scales of the DM interactions. We return to this question in Sec. V.

B. Discussion of the magnetization

The temperature, magnetic field, and concentration dependences of the magnetization in $Mn_{1-x}Fe_xSi$ and $Mn_{1-x}Co_xSi$ suggest the existence of an underlying ferromagnetic quantum critical point as described by the spin-fluctuation theory of itinerant electron ferromagnets. It is therefore instructive to consider the evolution of the phenomenological parameters A and b of this model defined in Eq. (1) when approaching the critical concentration. This also allows to discuss the possible concentration dependence of c and γ defined in Eq. (7) to be expected in future inelastic neutron scattering experiments.

Shown in Fig. 10 is the temperature dependence of the phenomenological parameters A and b derived from the ferromagnetic regime of the Arrott plots. The parameter A, which represents the inverse susceptibility, is negative below T_c and essentially linear as a function of temperature [Fig. 10(a)]. This is perfectly consistent with the behavior observed in weak itinerant ferromagnets such as $ZrZn_2$,[6,93] Ni_3Al, or $Pd_{1-x}Ni_x$.[94]

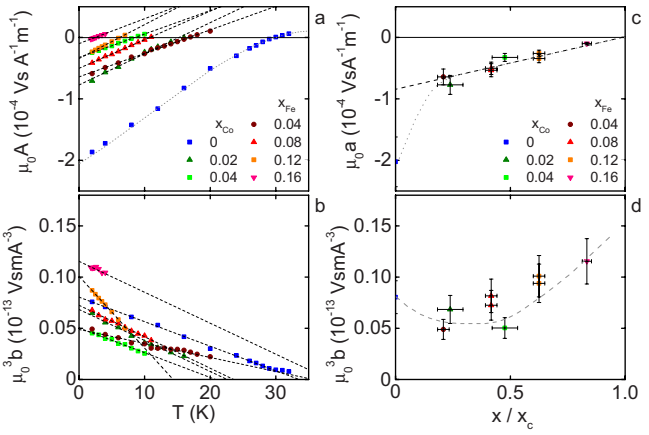

FIG. 10. (Color online) (a) Temperature dependence of the parameter A, the inverse susceptibility, inferred from the magnetization for various compositions of $Mn_{1-x}Fe_xSi$ and $Mn_{1-x}Co_xSi$. (b) Temperature dependence of the mode-coupling parameter b. (c) Extrapolated zero-temperature value of A as a function of normalized concentration x/x_c. (d) Extrapolated zero-temperature value of the mode-coupling parameter b as a function of normalized concentration x/x_c. The dashed lines are guides to the eyes.

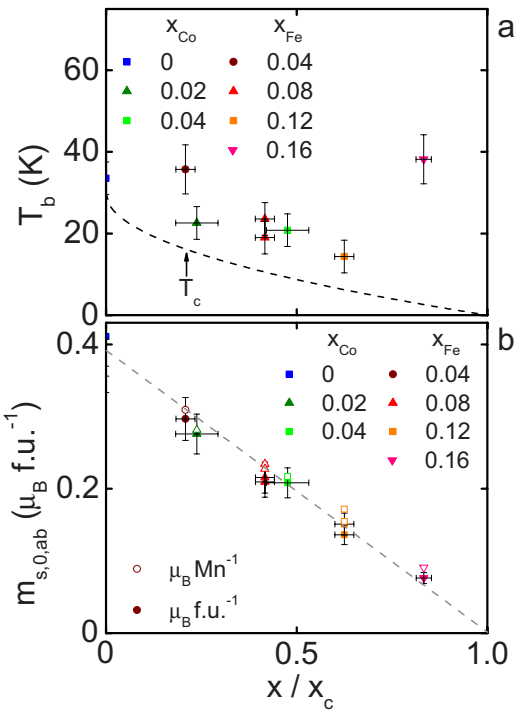

FIG. 11. (Color online) (a) Extrapolated temperature T_b of the change in sign from positive to negative of the mode-coupling parameter b inferred from the measured magnetization. (b) Ordered magnetic moment $m_{s,0,ab}$ calculated from the extrapolated zero-temperature value of the phenomenological parameters A and b. As a function of x the ordered moment decreases essentially linearly and extrapolates to zero for $x/x_c \to 1$.

Before turning to the variation in b with x it is helpful to discuss b inferred from pressure studies in MnSi. A negative value of b implies a first-order transition. A change from positive to negative is indeed implied in pure MnSi, when the helimagnetic transition changes from second order to first order for increasing pressure around $p^*=12$ kbar. As the simplest explanation, LDA band-structure calculations in MnSi suggest that the change of sign of b is due to a local minimum in the single-particle density of states near the Fermi level. However, there have been several proposals of more complex mechanisms driving b negative and the origin of the first-order transition under pressure has not been resolved yet.[10,11,13,14]

In addition, there has been a discussion for many years, whether pure MnSi displays a very weak first-order transition at ambient pressure (see, e.g., Refs. 95–97) alongside the strong evidence for first-order behavior in high-purity single crystals for pressures above p^* inferred from the observation of itinerant-electron metamagnetism. Most likely any faint features of first-order behavior at low pressures (which probe the domain populations of the helical state) and the tricritical point at high pressures are of different origin, the former being related to domain populations and the latter being related to overall features of the single-particle density of states. In fact, the first theoretical account of the helimagnetic order already predicted this transition to be first order.[33,34]

For $Mn_{1-x}Fe_xSi$ and $Mn_{1-x}Co_xSi$ we find that b is always positive. However, instead of being temperature independent b decreases with increasing temperature. Interestingly, when extrapolating the temperature dependence of b from low to high temperatures the parameter b appears to change sign at a temperature T_b that is always larger than T_c [Fig. 10(b)]. This suggests that the extrapolated transition at T_c stays second order for all compositions. In fact, we have observed similar temperature dependences of b in real weak itinerant ferromagnets such as $ZrZn_2$, Ni_3Al, or $Pd_{1-x}Ni_x$, though, to the best of our knowledge, they have not been discussed in the literature.

In spin-fluctuation theory the vicinity to a quantum critical point is typically controlled in terms of the zero-temperature value of the parameter $A(T \to 0)=a$ while all the other phenomenological parameters (b, c, and γ) are assumed to be essentially unchanged in the zero-temperature limit. Shown in Figs. 10(c) and 10(d) are the zero-temperature variation in a and b as a function of normalized concentration x/x_c. Following a rather strong initial increase in a between pure MnSi and the lowest doping levels, a increases linearly and extrapolates to zero for the critical concentration. This is consistent with a quantum critical point. Moreover, the mode-coupling parameter, b, is positive for all x and varies only relatively slowly [Fig. 10(d)]. This supports the possible existence of a quantum critical point at x_c.

Shown in Fig. 11(b) is the ordered moment calculated from the extrapolated zero-temperature values of A and b given as $m_{s,0,ab}=\sqrt{-a/b}$. Thus, even though the variation in T_c and m_s with x, shown in Figs. 7 and 8, seems unusual it is nevertheless consistent with the dependence of a and b on x and the concentration dependence of $m_{s,0}$. The evidence for an underlying ferromagnetic quantum critical point is also corroborated by the concentration dependence of T_b shown in Fig. 11(a). As mentioned above, for all concentrations studied $T_b > T_c$ suggesting that the extrapolated transition at T_c remains second order for $x \to x_c$.

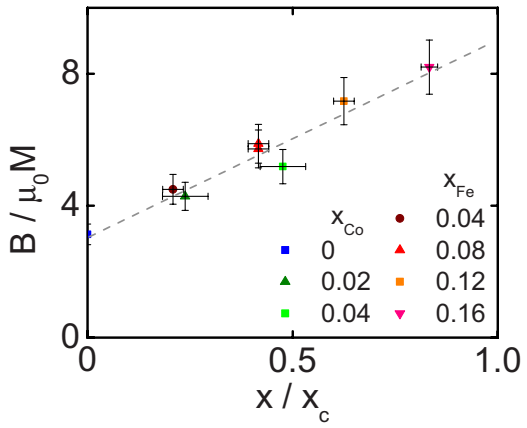

FIG. 12. (Color online) B/M as inferred from the Arrott plots in the conical phase. This quantity is equivalent to cQ^2, i.e., the product of spin-fluctuation stiffness with the square of the helimagnetic wave vector Q, see Eq. (18).

Several experimental studies of quantum critical points in complex f-electron compounds have suggested that a reduction in effective dimensionality of the spin excitations are at the heart of certain non-Fermi-liquid anomalies. The reduced dimensionality is thereby described in terms of anisotropies of the spin-fluctuation stiffness c. Without detailed microscopic measurements of the spin excitations it is not possible to clarify if the quantum critical spin fluctuations are anisotropic in $Mn_{1-x}Fe_xSi$ and $Mn_{1-x}Co_xSi$.

It is nevertheless interesting to speculate about the expected concentration dependence of the parameters c and $\hbar\gamma$ used to describe the spin-fluctuation spectra. As shown in the introduction, Eq. (18), the inverse linear susceptibility in the conical state, which increases linearly with increasing concentration, is given by cQ^2 (see Fig. 12). Small angle neutron scattering[77,82] at the same time shows that Q increases linearly with concentration. Shown in Fig. 13 are c and $\hbar\gamma$ as a function of the normalized concentration inferred from Eqs. (8) and (18) and the modulus of the magnetic ordering wave vector measured in neutron scattering (cf. Ref. 82).

Based on these considerations we expect a twofold decrease in the fluctuation stiffness c as shown in Fig. 13(a). The relaxation frequency spectrum $\Gamma(q)$ should hence display a more linear momentum dependence. Making use of Eq. (8) we also expect simultaneously an over tenfold increase in the energy spread $\hbar\gamma$ as shown in Fig. 13(b). This strong increase originates in the implicit dependence of T_c on $\hbar\gamma$ to the fourth power. Note, however, that the validity of Eq. (8) can be questioned because $m_{s,0}^2 - m_s^2 \propto T^2$ close to T_c, see Fig. 6, instead of the $T^{4/3}$ dependence expected for a critical ferromagnet. Nevertheless, Fig. 13(b) suggests a much stiffer relaxation frequency spectrum near the QPT. At a given temperature the spin fluctuations extend over a much smaller range of wave vectors.

We find both predictions surprising, since it is normally assumed that the parameters c and $\hbar\gamma$ remain unchanged when approaching a QPT. Detailed inelastic neutron-scattering studies are now needed to clarify whether the spin-fluctuation spectra near x_c are consistent with this prediction of spin-fluctuation theory and to what extent these parameters change with concentration x.

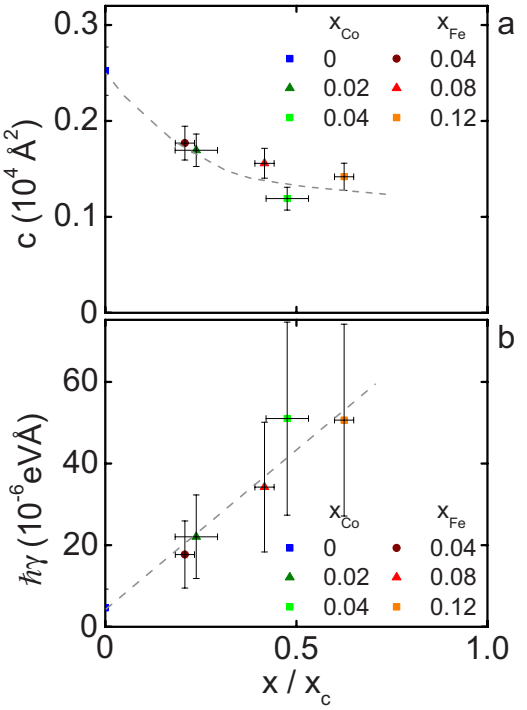

FIG. 13. (Color online) (a) The fluctuation stiffness c inferred from the linear susceptibility in the conical phase (horizontal line in the Arrott plot). Values are given in SI units (note that values given in Ref. 1 are given in cgs units). (b) Concentration dependence of the parameter γ describing the energy spread of the relaxation frequency spectra Γ, where γ was inferred from the expression of the Curie temperature in the spin-fluctuation theory, i.e., Eq. (8). Values are given in SI units (note that values given in Ref. 1 are given in cgs units).

V. AC SUSCEPTIBILITY

The magnetization so far provided foremost information on the ferromagnetic limit of the magnetic properties. Detailed information on modulated spin structures induced by the DM interactions may be inferred from the ac susceptibility. In particular, using the ac susceptibility we track in the following the evolution of the magnetic phase diagram as a function of composition.

A. Experimental results of the ac susceptibility

The temperature dependence of the ac susceptibility at various magnetic fields is shown in Fig. 14 for all compositions studied. In the paramagnetic state at high temperatures we observe for all x a pronounced Curie-Weiss dependence of the susceptibility characteristic of a large fluctuating moment m_{CW} [cf. Fig. 15(b)]. This high-temperature paramagnetic state provides the setting in which the low-temperature physics emerges. We return to a more detailed description of the high-temperature state further below.

At low temperatures the susceptibility displays a series of pronounced features characteristic of the helical phase, the conical phase, the A phase, and an intermediate regime (IM). Shown in Fig. 14(a) is the temperature dependence of the susceptibility of MnSi, which is in perfect agreement with

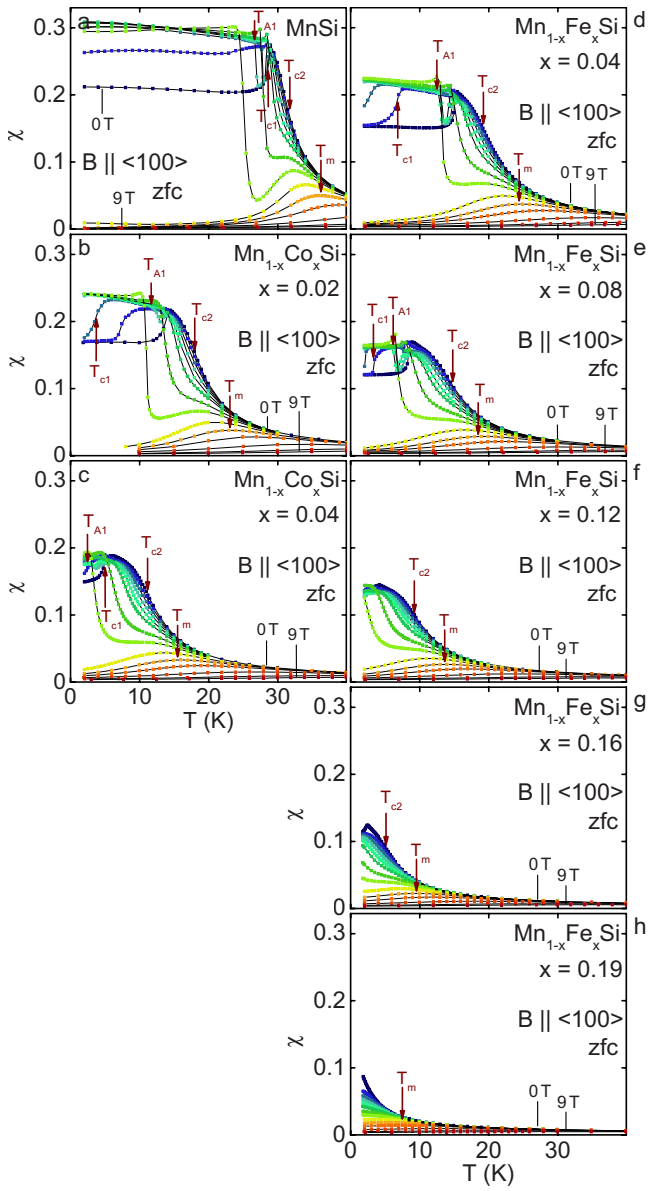

FIG. 14. (Color online) Temperature dependence of the ac susceptibility of MnSi, $Mn_{1-x}Co_xSi$, and $Mn_{1-x}Fe_xSi$. At high temperatures a pronounced Curie-Weiss dependence is observed. At low temperatures the characteristics of the various modulated spin structures are observed.

previous studies.[57,92] For $B=0$ the Curie-Weiss dependence is obeyed until close to the magnetic ordering temperature. We thereby define T_{c1} at the point of inflection of the susceptibility at low temperatures (see also Fig. 16), where we denote the zero-field limit as $T_1=T_{c1}(B\rightarrow 0)$.

We further define a characteristic temperature T_{c2} at the point of inflection of the susceptibility at the border to paramagnetism, where $T_{c2}>T_{c1}$, i.e., above T_{c2} the susceptibility displays the Curie-Weiss dependence. Again we denote the zero-field limit as $T_2=T_{c2}(B\rightarrow 0)$. We note that the transition temperature T_c, which was extrapolated from the magnetization in the ferromagnetic regime, is located between T_1 and T_2 for all compositions studied (green arrows in Figs. 21 and 22). Moreover, as will be shown below the temperatures T_1

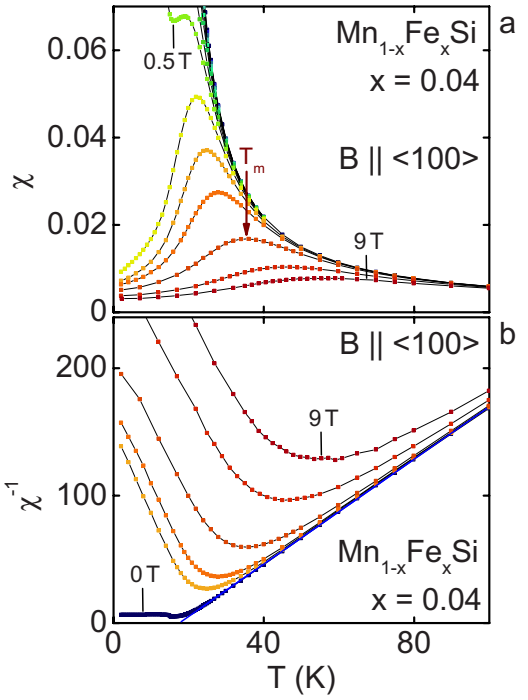

FIG. 15. (Color online) (a) ac susceptibility as a function of temperature for selected large applied magnetic fields. The maximum at temperature T_m represents the crossover between the field-polarized regime at low temperatures and high fields as opposed to the essentially paramagnetic regime at high temperatures and low fields. (b) Inverse susceptibility of the data shown in panel (a).

and T_2 correspond to features in the specific heat, notably a sharp maximum and a Vollhardt invariance. This means that there are clear thermodynamic signatures associated with these characteristic temperatures. As a final feature, for suitably chosen magnetic fields the susceptibility is slightly reduced in the temperature range of the A phase, where T_{A1} and T_{A2} are defined as lower and upper transition temperatures.

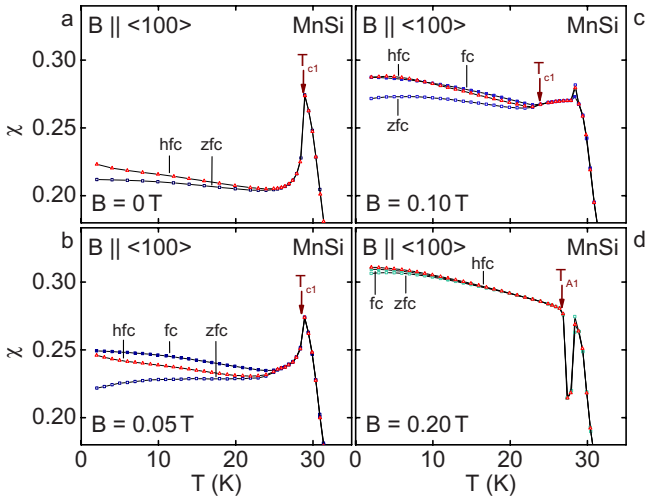

FIG. 16. (Color online) (a) Temperature dependence of the ac susceptibility of pure MnSi in zero magnetic field (a), $B=0.05$ T (b), $B=0.1$ T, (c) and $B=0.2$ T (d). Note the dip in panel (d), which is related to the A phase.

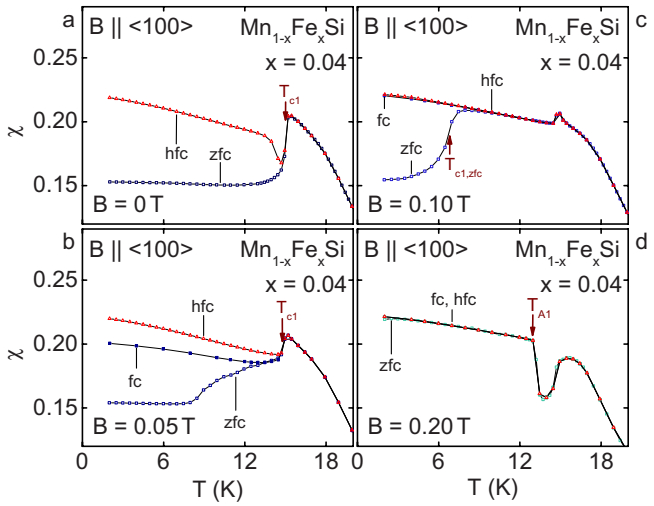

FIG. 17. (Color online) (a) Temperature dependence of the ac susceptibility of $Mn_{1-x}Fe_xSi$ ($x=0.04$) in (a) zero magnetic field, (b) $B=0.05$ T, (c) $B=0.1$ T, and (d) $B=0.2$ T. Note the dip in panel (d), which is related to the A phase.

For sufficiently large fields the susceptibility displays a broad maximum at the crossover between the field-polarized (ferromagnetic) state at low temperatures and high fields and the essentially paramagnetic state at high temperatures and low fields. A closeup view of this maximum in the susceptibility is shown for $Mn_{1-x}Fe_xSi$ and $x=0.04$ in Fig. 15(a). For fields $B<B_{c2}$ and decreasing temperature the maximum at T_m is followed by an abrupt increase when entering the conical phase. We return to the doping dependence of T_m below.

As a function of increasing Fe or Co content all features related to the helimagnetic state are shifted to lower temperatures and the Curie-Weiss dependence extents also to lower temperatures (Fig. 14). The total magnitude of the susceptibility thereby decreases and the quantitative changes in the susceptibility at the transition become less pronounced.

Differences of the temperature dependence of the ac susceptibility between zfc, fc, and hfc for pure MnSi are shown in Fig. 16. With decreasing temperature the susceptibility at zero magnetic field displays a sharp spike and drops to a reduced value [Fig. 16(a)]. With increasing field the susceptibility below T_{c1} increases and there is a small amount of hysteresis between fc and zfc visible at 0.05 and 0.1 T. For $B=0.2$ T a dip in the susceptibility is characteristic of the A phase.

Typical differences of the ac susceptibility as a function of temperature between zfc and hfc observed in $Mn_{1-x}Fe_xSi$ and $Mn_{1-x}Co_xSi$ are illustrated in Fig. 17, where the data shown were recorded for $Mn_{1-x}Fe_xSi$ and $x=0.04$. Overall the main features under doping are highly reminiscent of pure MnSi. In contrast with pure MnSi we find for all doped samples ($x\neq 0$) quite strong hysteresis for magnetic fields below 0.2 T. Moreover, the characteristic temperature below which the hysteresis occurs is also strongly field dependent and decreases rapidly with increasing temperature (see also phase diagrams shown in Figs. 21 and 22).

The magnetic field dependence of the ac susceptibility of pure MnSi and $Mn_{1-x}Fe_xSi$ for $x=0.08$ are shown in Figs. 18

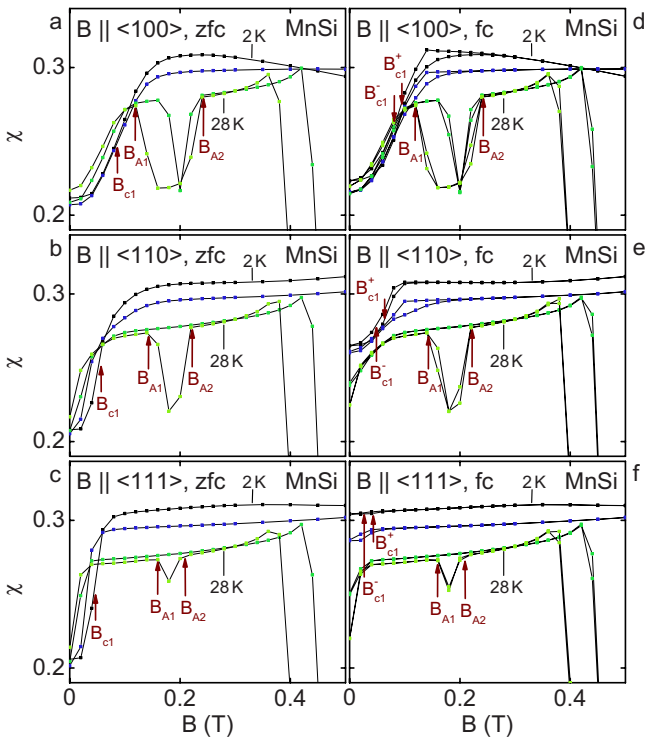

FIG. 18. (Color online) Magnetic field dependence of the susceptibility of pure MnSi for different field directions and selected temperatures. Under zfc conditions, shown in panels (a) through (c), the field B_{c1} decreases in the sequences ⟨100⟩, ⟨110⟩, and ⟨111⟩, consistent with the magnetic anisotropy. Under fc conditions, shown in panels (d) through (f), a similar trend may be observed. In the regime of the A phase the susceptibility displays a minimum of decreasing extent in the sequence ⟨100⟩, ⟨110⟩, and ⟨111⟩, again consistent with the magnetic anisotropy.

and 19 for different field directions and selected temperatures. As mentioned above our samples had the same cubic shape so that any demagnetizing effects for both samples and directions were the same. For each temperature data after initially zero-field-cooling and field-cooling are compared with a field sweep (FS) with decreasing field strength. Where available the data correspond very well with previous reports.[92,98] The characteristic fields are defined in strict correspondence with previous work in MnSi. Notably the point of inflection at B_{c1} marks the transition from the helical state to the conical state, where we find a small amount of hysteresis. We denote the zero-temperature limit as $B_1=B_{c1}(T\rightarrow 0)$. The upper critical field B_{c2} is defined at the point of inflection of the decreasing susceptibility, where $B_2=B_{c2}(T\rightarrow 0)$. The transition fields B_{A1} and B_{A2} of the A phase are defined at the boundaries of the regime of reduced susceptibility.

As a function of orientation the salient features in pure MnSi are twofold. First, the field value of the reorientation B_{c1} decreases as a function of orientation in the order ⟨100⟩, ⟨110⟩, and ⟨111⟩ [Figs. 18(a)–18(c)]. For the zfc state the helical state at $B=0$ is more pronounced than for fc. Second, the size of the signal reduction and the extent in the B versus T diagram of the A phase decreases as a function of orientation in the order ⟨100⟩, ⟨110⟩, and ⟨111⟩ [Figs. 19(d)–19(f)].

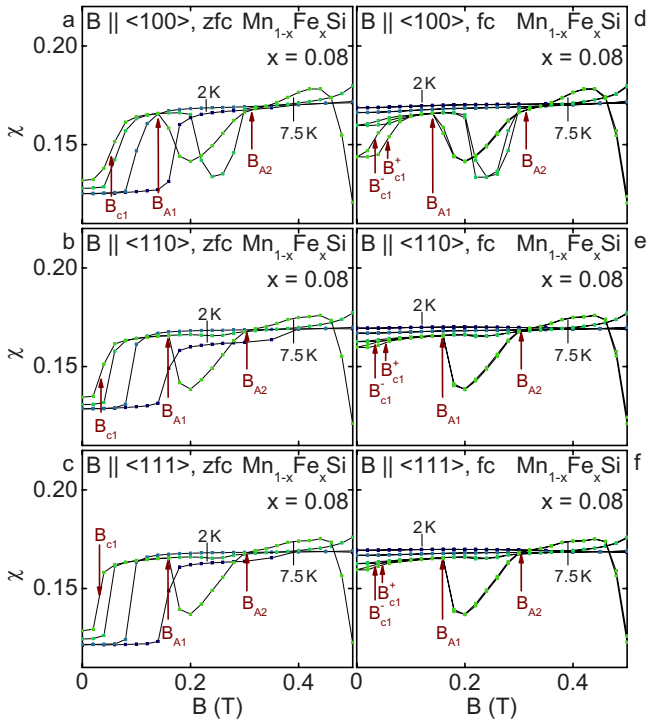

FIG. 19. (Color online) Magnetic field dependence of the susceptibility of $Mn_{1-x}Fe_xSi$ for $x=0.08$ for different field directions and selected temperatures. Under zfc conditions the field B_{c1} does not change much between ⟨100⟩, ⟨110⟩, and ⟨111⟩, consistent with a reduced magnetic anisotropy as compared with MnSi. Under fc conditions the same trend may be observed, i.e., less anisotropy. Likewise the extent of the signal in the A phase does not change much.

Under doping these salient features change in the following manner. For zfc the field value of the reorientation at B_{c1} is essentially unchanged for ⟨100⟩, ⟨110⟩, and ⟨111⟩. However, for fc the helical order at $B=0$ is essentially no longer recovered.

The data of MnSi reflect the magnetic anisotropy, i.e., differences of pinning potential for the helical order. For field parallel to ⟨111⟩, which is the easy axis, the spin-flop transition into the conical state occurs at the lowest value of B_{c1} while the value of B_{c1} is largest for ⟨100⟩, which is the hard axis. In the same way differences of the A phase are consistent with the magnetic anisotropy, where the extent of the A phase is largest for the hard axis. The differences in field range of the A phase are strongly reduced or even lost in $Mn_{1-x}Fe_xSi$ ($x=0.08$) as opposed to the temperature range which is still largest for a ⟨100⟩ direction. Thus a dominant effect of the doping must be the reduction in the magnetic anisotropy. At the same time $B_{c1,zfc}$ remains high, i.e., there is no reduction in the magnetic anisotropy with increasing concentration.

As a second trend there is increasing hysteresis between zfc and fc. This is especially reflected in the temperature dependence of B_{c1}, which is much higher and decreases linearly with increasing temperature in doped samples (cf. Figs. 21 and 22). Likewise the changes in the susceptibility in the fc data suggest that the helical state may even get not recovered for $B<B_{c1}$. This behavior is strongly reminiscent of the phase diagrams observed in $Fe_{1-x}Co_xSi$.[48] The hysteresis may be readily explained with local minima of a glassy energy landscape due to disorder introduced by the doping that competes with the magnetic anisotropy. The size of these local minima must be similar to the magnetic anisotropy. For increasing temperature thermal excitations assist the magnetic order in a zfc state to return to the direction favored by the magnetic field direction. In contrast, for a fc state the pinning is strong enough to stay in the field direction, so that the magnetic anisotropy is not sufficient to reorient the magnetic order.

Typical magnetic field dependences of the ac susceptibility for all concentrations studied are summarized in Fig. 20. For clarity the data have been shifted vertically. The data shown here have been recorded in field cycles from $B=-1$ T to $B=+1$ T and back to $B=-1$ T. This complements the zero-field-cooled data shown in Fig. 14. Representative examples for the features that define the transition fields are marked by arrows. The reduction in the susceptibility in the A phase persists under doping and may be traced almost all the way to the critical concentration. With increasing concentration x the signatures of the helical state and the A phase become less pronounced, notably the size of the reduction in the susceptibility in the helical and A phase as compared with the conical phase decreases. In fact, for $Mn_{1-x}Fe_xSi$ with $x=0.12$ the evidence for the A phase is extremely shallow, raising the question if an A phase forms at all. We can no longer identify a feature that would suggest the existence of an A phase for $Mn_{1-x}Fe_xSi$ and $x=0.16$ down to lowest temperature measured of ~ 1.8 K.

The magnetic phase diagrams of MnSi, $Mn_{1-x}Co_xSi$, and $Mn_{1-x}Fe_xSi$ after zero-field cooling and field cooling are shown in Figs. 21 and 22, respectively. In the following we distinguish six regimes as conveniently identified in pure MnSi, where the magnetic structure is known from neutron scattering: (i) the paramagnetic state at high temperatures and low fields (no shading); (ii) the spontaneously ordered helimagnetic phase (blue shading); (iii) the conical phase in which the propagation vector of the helical modulation is aligned parallel to the applied magnetic field (gray shading); (iv) the A phase just below T_c which was recently identified as a skyrmion lattice (red shading); (v) an intermediate regime (purple shading), and (vi) the field-polarized ferromagnetic phase at low temperatures and high fields.

The phase boundaries of the various phases are defined as follows. Data points at the boundary of the helical order are denoted as T_{c1} and B_{c1}. Data points separating the paramagnetic and field-polarized ferromagnetic states (no shading) from the modulated phases at low temperatures and low fields are denoted as T_{c2} and B_{c2}, where T_m marks the crossover between the paramagnetic and the field-polarized (ferromagnetic) regime. The A phase is bounded by T_{A1}, T_{A2}, B_{A1}, and B_{A2}, respectively. These definitions of the phase boundaries are supported by the specific heat as discussed below. In particular, with decreasing temperature we find a Vollhardt invariance at the onset of the intermediate regime at T_2 and a spike in the specific heat at the onset of the helimagnetic order at T_1. This spike in the specific heat also denotes the line separating the intermediate regime from the conical and A phase.

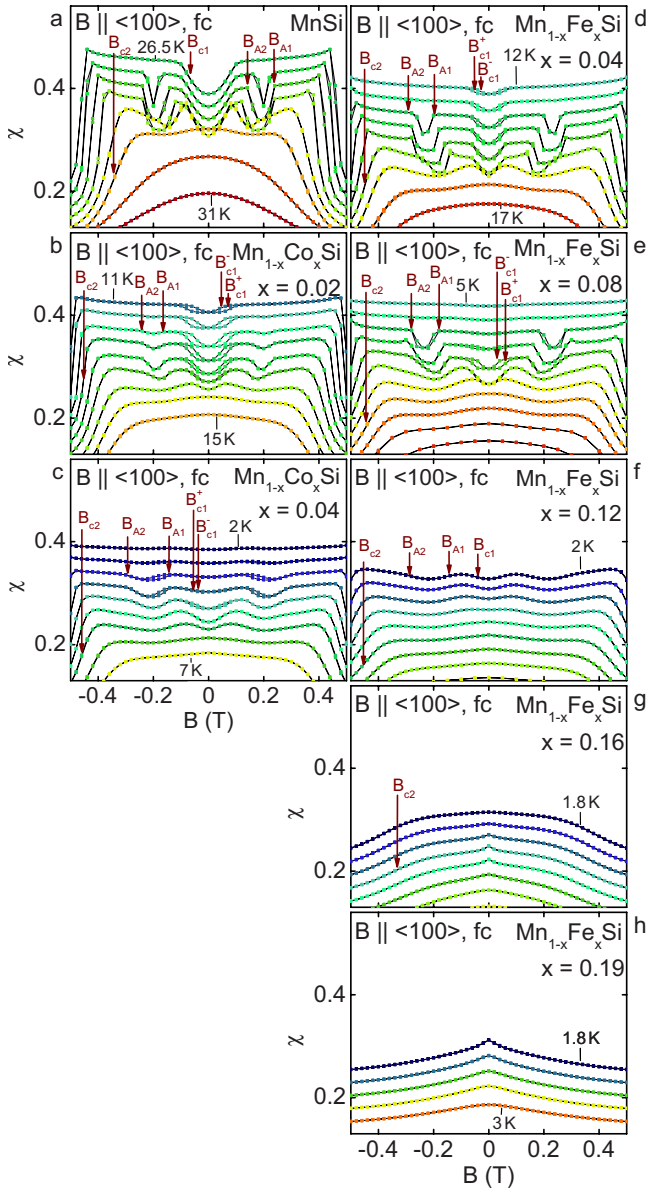

FIG. 20. (Color online) Magnetic field dependence of the ac susceptibility of MnSi, $Mn_{1-x}Co_xSi$, and $Mn_{1-x}Fe_xSi$ at selected temperatures. Data have been recorded in field cycles from −1 T to +1 T and back, thus reflecting the properties of the field-cooled state.

The magnetic phase diagrams after zero-field cooling and field cooling actually agree remarkably well, except for the phase boundary of the zero-field-cooled helimagnetic state in the doped samples. In particular, the strongly temperature-dependent transition line of the helimagnetic state after zero-field cooling for all $x \neq 0$ agrees qualitatively very well with the magnetic phase diagram we recently observed in $Fe_{1-x}Co_xSi$.[48]

As a final remark in this section we note that it is surprising to find $T_1 < T_c$. Based on the hierarchy of energy scales one would expect that T_1 is always larger than the underlying ferromagnetic transition temperature T_c as the transition to the helical state at T_1 preempts the ferromagnetic transition. As we find $T_1 < T_c$ for all concentrations, this relation seems

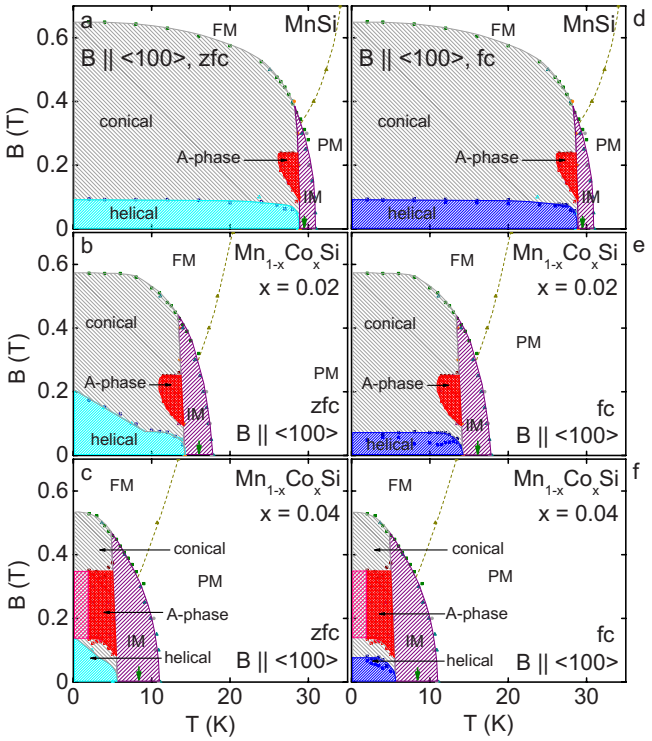

FIG. 21. (Color online) Magnetic phase diagram of MnSi and $Mn_{1-x}Co_xSi$ after zero-field cooling and field cooling. We distinguish six regimes: (i) paramagnetism at high temperatures and low fields, (ii) spontaneous helimagnetism (blue shading), (iii) the conical phase (gray shading), (iv) the A phase (red shading), (v) an intermediate regime (purple shading), and (vi) the field-polarized ferromagnetic regime. The shading is extended down to zero temperature, where the lowest temperature studied was ~1.8 K. The green arrows mark the location of the extrapolated ferromagnetic transition temperature T_c. The dashed line marks the location of T_m.

to be systematic for T_c as inferred from the Arrott plots. In contrast, the expected relation $T_m < T_1$ is satisfied by the crossover temperature T_m after extrapolation to zero magnetic field. We discuss these findings in more detail below.

B. Discussion of the ac susceptibility

In the following we return at first to a discussion of the ferromagnetic regime of the magnetization and the information we inferred from the magnetization data. We thereby compare the ac susceptibility with the properties expected in the spin-fluctuation theory of weak itinerant ferromagnetism. This is followed by a discussion of the zero-field temperature versus concentration phase diagram in the presence of the DM interactions.

In spin-fluctuation theory of three-dimensional itinerant-electron ferromagnets the vicinity to a QCP is determined by the inverse initial (T=0) susceptibility given by the parameter a_0. The other three parameters of the model (b, c, and γ) are assumed to remain unchanged. Consequently the fluctuating Curie-Weiss moment at high temperatures is expected to remain unchanged when approaching a quantum critical point. In Sec. IV we have shown that the magnetization provides strong evidence of an underlying ferromagnetic quan-

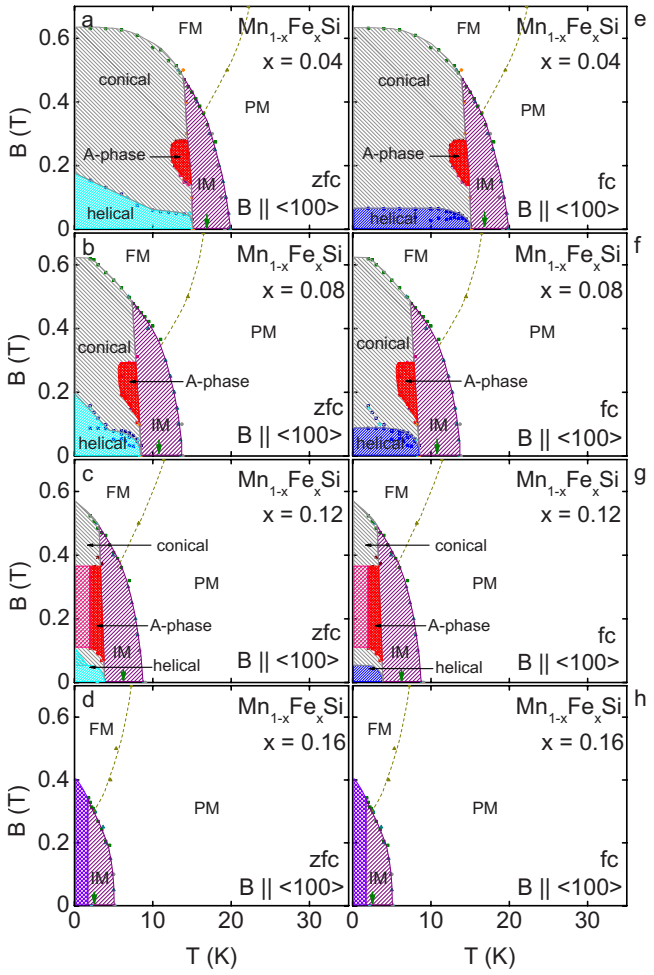

FIG. 22. (Color online) Magnetic phase diagram of $Mn_{1-x}Fe_xSi$ after zero-field cooling and field cooling. We distinguish six regimes as explained in the text and the caption of Fig. 21. The phase diagram for field cooling agrees very well with the phase diagram after zero-field cooling, except for the phase boundary of the spontaneous helimagnetic order (blue shading) in all doped samples ($x \neq 0$). The shading is extended down to zero temperature, where the lowest temperature studied was ~1.8 K. The green arrows mark the location of the extrapolated ferromagnetic transition temperature T_c. The dashed line marks the location of T_m.

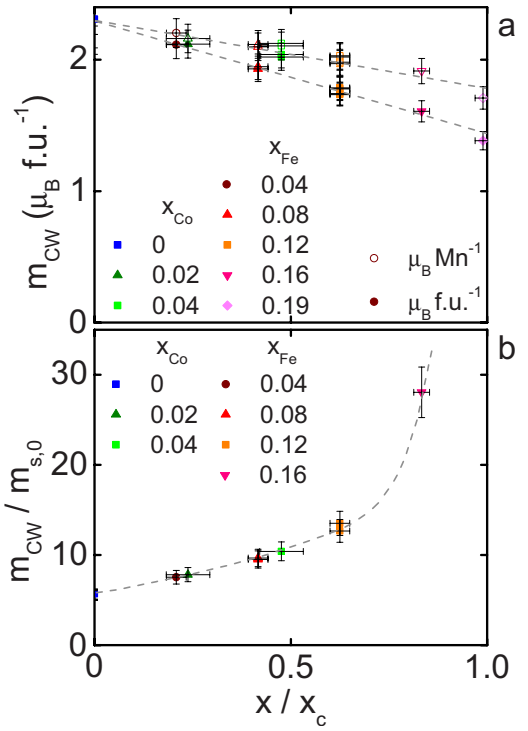

FIG. 23. (Color online) (a) Curie-Weiss moment of the paramagnetic state as a function of normalized composition x/x_c. (b) Ratio of the effective Curie-Weiss moment to the ordered moment inferred from the measured magnetization.

tum critical point under Fe or Co doping of MnSi. It is therefore interesting to consider at first the evolution of the Curie-Weiss dependence in $Mn_{1-x}Fe_xSi$ and $Mn_{1-x}Co_xSi$

As shown in Fig. 23(a) the Curie-Weiss moment of $Mn_{1-x}Fe_xSi$ and $Mn_{1-x}Co_xSi$ decreases as a function of normalized composition x/x_c by about ~30% at x_c [see also Fig. 15(b)]. Even though this decrease is quite weak, it is clearly outside standard spin-fluctuation theory. In order to explore if the reduction originates in the reduction in the number of Mn atoms in the composition we have also calculated the effective Curie-Weiss moment per Mn atom, i.e., the fluctuating Curie-Weiss moments are entirely attributed to the Mn atoms. The effective moment inferred this way nevertheless decreases linearly as a function of composition, even though not as fast as the average moment. This suggests that the Curie-Weiss moment originates also in the Fe and Co ions and the spin fluctuations are itinerant as for pure MnSi.

Further, a hallmark of weak itinerant ferromagnetism is the strongly reduced ordered moment as compared with the fluctuating Curie-Weiss moment. Since the Curie-Weiss moment decreases somewhat with increasing x we have also considered the ratio of Curie-Weiss moment to the extrapolated ordered moment shown in Fig. 23(b). For increasing x this ratio increases and appears to diverge as expected. Of course this divergence is dominantly the result of the reduction in $m_{s,0}$, which must be faster than the reduction in the effective Curie-Weiss moment.

Next the Curie-Weiss dependence of the susceptibility in the paramagnetic regime may be used to obtain an alternative estimate of the initial susceptibility as a function of normalized concentration shown in Fig. 24. This figure may be compared with the initial susceptibility inferred from the magnetization shown in Fig. 10(c) depicted as black dashed line in Fig. 24. Interestingly the initial susceptibility inferred from the ac susceptibility in the paramagnetic regime is linear over the entire range of compositions, i.e., the value for $x=0$ is consistent with all compositions. Further, consistent with Fig. 10(c) the inverse initial susceptibility extrapolates to zero for $x/x_c \rightarrow 1$. However, as an unresolved issue the initial susceptibility inferred from the Curie-Weiss susceptibility in the paramagnetic regime is quantitatively roughly 30% smaller than that inferred from the magnetization at low temperatures. This type of inconsistency is not uncommon amongst weakly ferromagnetic materials. Its resolution awaits fresh theoretical input.

Shown in Fig. 25 are the characteristic transition fields as a function of the normalized composition inferred from the

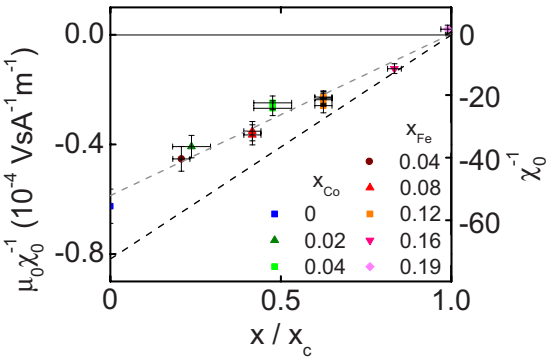

FIG. 24. (Color online) Zero-temperature inverse susceptibility as inferred from the Curie-Weiss dependence of the ac susceptibility versus normalized concentration. This quantity extrapolates to zero at the critical concentration ($x/x_c \to 1$). The lower dashed line indicates the same property inferred from the field dependence of the magnetization [Fig. 10(c)], which also extrapolates to zero for $x/x_c \to 1$. The quantitative difference between ac susceptibility and magnetization based data are unexplained.

susceptibility measurements. Toward the critical concentration the zero-temperature values of the upper critical fields B_2 decreases substantially. As explained in the introduction, Eq. (20), the upper critical field may be calculated from the measured linear susceptibility in the conical phase [giving cQ^2, see Eq. (18)] and the parameters a and b of the Ginzburg-Landau potential. Using for the latter the values extracted from the Arrott plots, see Eq. (21), we calculate values for B_2 (open symbols in Fig. 25) that are in remarkable agreement with the ones measured directly in the ac susceptibility. Similarly, we expect a temperature dependence of

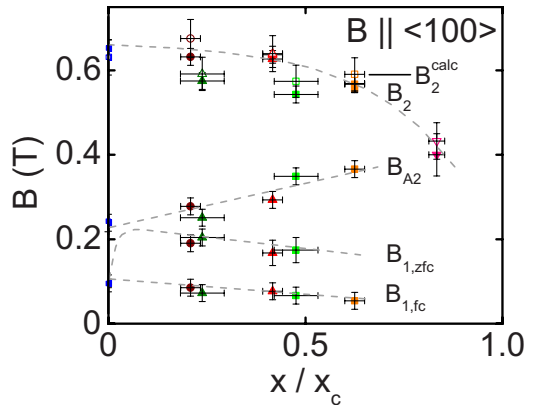

FIG. 25. (Color online) Transition fields versus normalized concentration of $Mn_{1-x}Fe_xSi$ and $Mn_{1-x}Co_xSi$. The upper critical field appears to collapse towards the critical concentration. For comparison also included are the calculated values of B_2^{calc} using Eq. (20) (open symbols), which are in remarkable agreement with the values of B_2 measured in the ac susceptibility. We distinguish two lower critical fields as determined in zfc and fc conditions. The weak concentration dependence of $B_{1,zfc}$, which reflects the magnetic anisotropy, could only be determined up to $x/x_c \approx 0.5$. It suggests that the QPT may not be driven by an unpinning of the helical order.

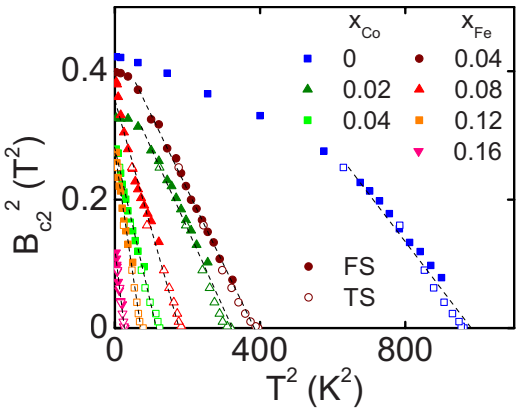

FIG. 26. (Color online) Upper critical field squared, B_{c2}^2, versus temperature squared. As expected a linear relationship is observed over a wide range. FS and TS denote data points inferred from field and temperature sweeps, respectively.

$$B_{c2} = cQ^2 \sqrt{\frac{cQ^2 - a}{b}} \tag{22}$$

that is essentially given by the extrapolated magnetic moment $m_s^2 = -a/b$. This is borne out in Fig. 26 where it is demonstrated that B_{c2}^2 inherits the T^2 temperature dependence of m_s^2, see Fig. 6.

Concerning the lower critical field we distinguish B_1 as measured in zfc conditions from that measured in fc conditions, see Fig. 25. In comparison to B_2 both lower critical fields, $B_{1,zfc}$ and $B_{1,fc}$, decrease only weakly under Co and Fe doping, where $B_{1,fc}$ might extrapolate to zero for $x \to x_c$. However, $B_{1,zfc}$ reflects the magnetic anisotropy while $B_{1,fc}$ results from the combination of disorder and magnetic anisotropy. Hence our study suggests that the strength of the magnetic anisotropy is only affected weakly by Co and Fe doping when approaching the critical concentration. Thus, unlike earlier reports, notably Ref. 77, the QPT in $Mn_{1-x}Fe_xSi$ and $Mn_{1-x}Co_xSi$ may not be driven by an unpinning of the helical order (note that $B_{1,zfc}$ could only be determined up to $x/x_c \approx 0.5$). The same conclusion was reached in the small angle neutron-scattering study of the pressure-induced suppression of helical order in pure MnSi, cf. Ref. 59, where B_1 was found to be essentially unchanged under pressure.

It is finally interesting to note that the upper critical field of the A phase, B_{A2}, increases as shown in Fig. 25 (it is not possible to obtain an estimate of B_{A1} suitable for Fig. 25). This suggests that the A phase becomes more extended when moving toward the quantum critical point. The simultaneous loss of the signature of the A phase in the ac susceptibility additionally suggests that the various magnetic phases cannot be distinguished any longer. This conjecture is supported by our small angle neutron scattering studies to be reported elsewhere.[82]

We next return to the temperature and magnetic field dependences of the maximum in the susceptibility at T_m shown in Fig. 27. Empirically it is clear that T_m separates the field-polarized ferromagnetic regime at low temperatures and high fields from the paramagnetic regime at high temperatures and low fields. It is possible to compare the doping depen-

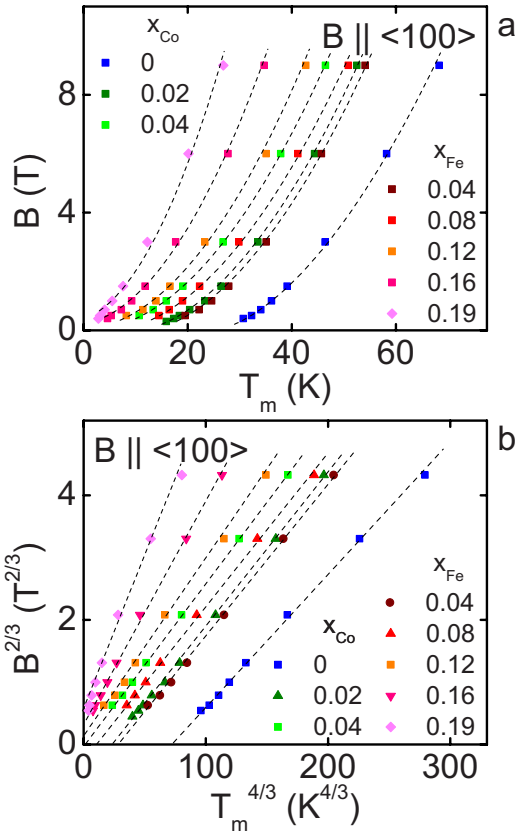

FIG. 27. (Color online) Crossover temperature T_m between the field-polarized ferromagnetic regime and paramagnetic regime for various compositions as plotted on a temperature scale to the 4/3 and a magnetic field scale 2/3. The quasilinear dependence for various x is consistent with ferromagnetic quantum criticality underlying the properties of $Mn_{1-x}Fe_xSi$ and $Mn_{1-x}Co_xSi$.

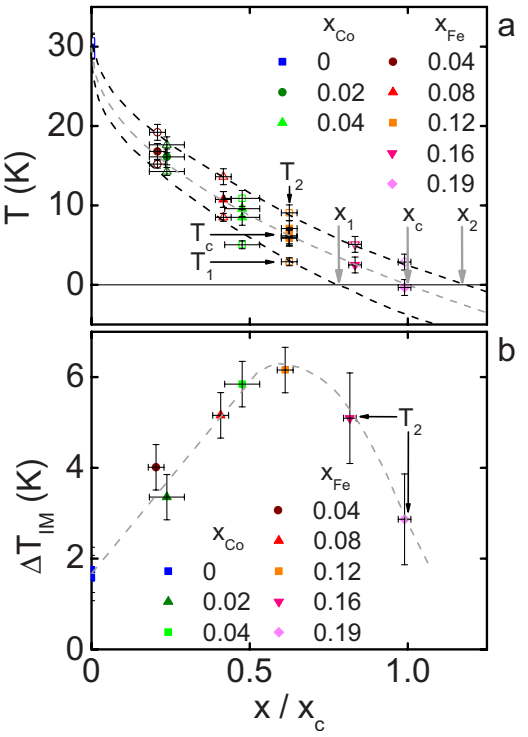

FIG. 28. (Color online) (a) Temperature versus composition phase diagram summarizing the characteristic transition temperatures inferred from the ac susceptibility. Also shown are the transition temperatures inferred from the magnetization (cf. Fig. 7). (b) Difference ΔT_{IM} between the temperatures T_1 and T_2 as a function of composition. This represents the zero-field temperature range of the intermediate regime in the magnetic phase diagram.

dence of T_m with the predictions of spin-fluctuation theory.

The crossover between the two regimes is captured by the equation of state Eq. (1) with positive coefficient $A(T)>0$. Whereas in the field-polarized regime the magnetization depends nonanalytically on the magnetic field, $M \approx (B/b)^{1/3}$, its dependence is linear in the paramagnetic regime, $M \approx B/A$. The crossover occurs for magnetic fields of order $B \sim A(T_m)^{3/2}/\sqrt{b}$. When plotting $B^{2/3}$ versus $T_m^{4/3}$ we find a linear relationship for all concentrations as shown in Fig. 27(b). Such a behavior is expected for renormalizations by critical ferromagnetic fluctuations that yield a $T^{4/3}$ temperature dependence for $A(T)$. However, as a consequence of this argument one expects that $T_m|_{B\to 0} \to 0$ for $x \to x_c$. In comparison, the experimentally observed values of $T_m|_{B\to 0}$ decrease faster and vanish already for doping concentrations $x<x_c$ that are smaller than the critical concentrations, x_c, extracted from extrapolations of the Arrott plots, see Fig. 6.

A summary of the transition temperatures inferred from the ac susceptibility and the magnetization versus normalized composition x/x_c is shown in Fig. 28(a). Both T_1 and T_2 decrease monotonically and appear to vanish above x_1 and x_2, respectively. For $T_1 \to 0$ this results in a putative QPT between helimagnetic order and the spin state of the intermediate regime. For increasing composition this is followed by $T_2 \to 0$, which represents a zero-temperature crossover between the spin state of the intermediate regime and the paramagnetic state. The critical concentrations for Fe doping are roughly $x_1^{Fe} \approx 0.151$ and $x_2^{Fe} \approx 0.225$ and for Co doping roughly $x_1^{Co} \approx 0.066$ and $x_2^{Co} \approx 0.099$. As a function of normalized concentration x/x_c this corresponds under Fe and Co doping to the same normalized values $x_1/x_c \approx 0.78$ and $x_2/x_c \approx 1.17$. Taken together these data suggest the possible existence of a quantum phase transitions, where the regime for $x>x_1$ is separated further by the Vollhardt invariance. This is supported further by the difference $\Delta T_{IM}=T_2-T_1$ as shown for increasing x/x_c in Fig. 28(b).

Our data on the various crossover and transition temperatures have some apparently puzzling implications. For all concentrations the extrapolated ferromagnetic transition temperature T_c, inferred from the magnetization resides between T_1 and T_2, i.e., the critical concentration of the underlying ferromagnetic quantum critical point is located between the putative QPT at T_1 of the helimagnetic order and the point of suppression of the intermediate regime at T_2, $T_1<T_c<T_2$. This is surprising as one would expect T_1 to be smaller than a ferromagnetic transition temperature as the transition into the helical phase preempts ferromagnetism. The crossover temperature T_m extrapolated to zero magnetic fields, on the other hand, obeys $T_m<T_1$ as expected.

One might be tempted to attribute the relation $T_1<T_c$ to a systematic error in the analysis of the Arrott plots, for example, due to the residual dependence of the A parameter in

Eq. (21) on the Dzyaloshinsky-Moriya interaction via the magnetization M_{c2}. However, whereas this residual dependence becomes negligible in the low-temperature limit, the relation $T_1 < T_c$ is consistently observed up to high doping values where both transition temperatures vanish at doping concentrations x_1 and x_c, respectively, with $x_1 < x_c$. Nevertheless, we suggest that this discrepancy might be resolved by taking into account the strong fluctuations that accompany the transition into the helical phase. An analysis of the Goldstone spectrum[99] shows that $d=3$ is the lower critical dimension for an isotropic helical magnet so that helical order, in fact, cannot exist at finite temperatures without anisotropies. The helical phase observed is thus only stabilized by small anisotropy energies resulting in a suppression of the helical transition temperature T_1 as compared to its mean-field estimate. This may explain the observed relation $T_1 < T_c$.

Our experimental results suggest a rather interesting new scenario, in which two weak energy scales, notably the magnetic anisotropy of the helimagnetic order (as affected by disorder) and the DM interaction causing the helical modulation, surround an underlying ferromagnetic quantum critical point which seems to drive the QPTs of these weak scales. In contrast, for pure MnSi it has been suggested that pressure causes a consecutive collapse of the three hierarchical energy scales. In other words, for increasing pressure there are quantum phase transitions starting with the weakest scale (the magnetic anisotropy) at lowest pressure and finishing with the strongest scale (the ferromagnetic stiffness) at the highest pressure.[59,60]

VI. SPECIFIC HEAT

The specific heat further qualifies the magnetic phase diagrams derived from the magnetization and susceptibility. We will first address the thermodynamic evidence of the transitions at T_1 and the crossover at T_2, and the consistency of the electronic contributions of the specific heat with quantum criticality. In the discussion we then turn to the entropy as a function of composition.

A. Experimental results of the specific heat

Shown in Figs. 29(a) and 29(d) is the temperature dependence of the specific heat of pure MnSi up to 35 K for various magnetic fields. The paramagnetic to helimagnetic transition is accompanied by a pronounced anomaly. Detailed inspection of this anomaly reveals additional structure. With decreasing temperature at first a shoulder emerges, followed by a sharp spike. These data are in excellent agreement with previous studies.[96,100,101] In fact, the observation of this feature, first reported in Ref. 101, inspired theoretical work concerning the question of a spontaneous skyrmion ground states in chiral magnets[61] (see also discussion in online supporting material of Ref. 61). The proposal of a spontaneous skyrmion phase has recently been studied in spin-echo neutron scattering,[102] where the same authors come to differing conclusions of their data,[103] strongly suggesting that the situation at present is inconclusive.

Two characteristic temperatures may be defined in the specific heat of MnSi. First, the sharp spike in the specific

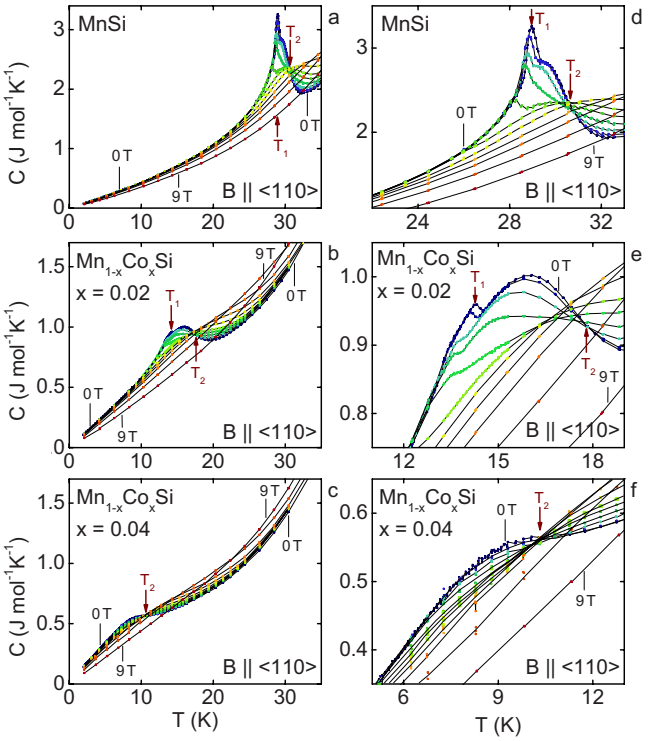

FIG. 29. (Color online) Specific heat of pure MnSi and $Mn_{1-x}Co_xSi$ as a function of temperature. Panels (a)–(c) show an overview up to 35 K. Panels (d)–(f) show a closeup view of the specific heat of pure MnSi and $Mn_{1-x}Co_xSi$ in the vicinity of the magnetic phase transition, highlighting the Vollhardt invariance at T_2, and the spike at T_1.

heat corresponds very well with T_1 defined in the ac susceptibility. It further turns out that the point of inflection in the specific heat corresponds very well with the temperature T_2 determined in the ac susceptibility. We will see below, that these definitions actually also apply in $Mn_{1-x}Fe_xSi$ and $Mn_{1-x}Co_xSi$.

The magnetic field dependence provides key information as to the nature of the features at T_1 and T_2, respectively. The spike in the specific heat at T_1 is characteristic of the latent heat of a weak first-order transition (the slight broadening may be due to defects in the sample and the heat-pulse method used in the measurements). As a function of magnetic field the feature at T_1 rapidly broadens, shifts to lower temperatures and vanishes above around 0.4 T.

For magnetic fields up to ~ 0.5 T the inflection point of all specific-heat curves at T_2 coincide at the same value of $C=2.3$ J mol^{-1} K^{-1}, i.e., $\partial C(T)/\partial B=0$. This is the characteristic of a Vollhardt invariance.[80,81] The parameter range over which the Vollhardt invariance may be observed provides evidence of characteristic energy scales of the system. In MnSi the invariant crossing in the specific heat indeed coincides with the turning point in the susceptibility at T_2.[100] Thus, the shoulder in C is the consequence of an important intrinsic energy scale of the system. The magnetic field range over which the Vollhardt invariance is observed identifies this energy scale as the DM interactions.

It is now helpful to locate the magnetic field dependence of T_{c1} and T_{c2} in the magnetic phase diagram. In the zero-

field limit T_2 and the upper critical field B_{c2}, as inferred from the point of inflection in the magnetic field dependence in the susceptibility, emerge from the same line. This is not surprising, since T_2 and B_{c2} are both due to the DM interactions. The maximum in the specific heat at T_1, on the other hand, increases very steeply under field and eventually merges with the B_{c2}.

It is instructive to compare the specific heat of pure MnSi with the properties observed in $Mn_{1-x}Co_xSi$ for $x=0.02$ shown in Figs. 29(b) and 29(e). For decreasing temperature in zero magnetic field the transition is still characterized by a broad shoulder followed by a tiny spike. In comparison to pure MnSi the shoulder is broadened while the peak is very small. Under applied magnetic fields the point of inflection of the specific heat is again unchanged, representing a Vollhardt invariance up to 0.5 T. The small spike at T_1 broadens and turns into a cusp, which eventually merges with the upper critical field B_{c2}. Taken together, this behavior is strongly reminiscent of pure MnSi. For $Mn_{1-x}Co_xSi$ with $x=0.04$, shown in Figs. 29(c) and 29(f), only the shoulder remains, but the narrow spike has completely vanished. Under magnetic field the point of inflection at T_2 is again invariant up to 0.5 T.

Shown in Fig. 30 is the specific heat of $Mn_{1-x}Fe_xSi$ for Fe concentrations of $x=0.04$, 0.08, 0.12, 0.16, and 0.19. The Fe-doped system exhibits the same key features as observed in the Co-doped system, notably a spike at T_1 at low Fe concentrations that becomes smaller and a Vollhardt invariance at a temperature T_2 for magnetic fields up to 0.5 T. For high Fe concentrations the feature at T_1 vanishes and the specific heat is dominated by the broad maximum. As mentioned above, in the magnetic phase diagram we define the separation line between the intermediated regime (IM) and conical phase or A phase at the spike in the specific heat.

We have analyzed the temperature dependence of the specific heat further, estimating the lattice contribution at high temperatures in the framework of a standard Debye model. The estimate is illustrated in Fig. 31, where the specific heat shown is that of $Mn_{1-x}Fe_xSi$ for $x=0.04$. Also shown is the full Debye dependence (green) and the approximate cubic temperature dependence of the Debye dependence at low temperatures (red). The Debye dependence is thereby determined at high temperatures by fixing the Debye temperature as the only fit parameter; for $x=0.04$ we find $\Theta=512$ K. As shown in Figs. 31(a) and 31(c) the full Debye dependence up to ~50 K differs by not more than a few percent from the approximate cubic low-temperature form. The lattice subtraction used here finds further support in the temperature dependence of the specific heat above T_2, where a cubic temperature dependence as expected for the Debye model is observed [Figs. 31(b) and 31(d)]. We have therefore subtracted in the following lattice contributions using the cubic approximation.

Across the series of Fe- and Co-doped compounds the Debye temperature is essentially unchanged as shown in Fig. 32. In particular, the Debye temperature is unchanged as compared with pure MnSi, where the temperature range in which the magnetic properties dominate is less than 10% of Θ. This is consistent with the cubic approximation of the lattice contributions. In the following we assumed that the

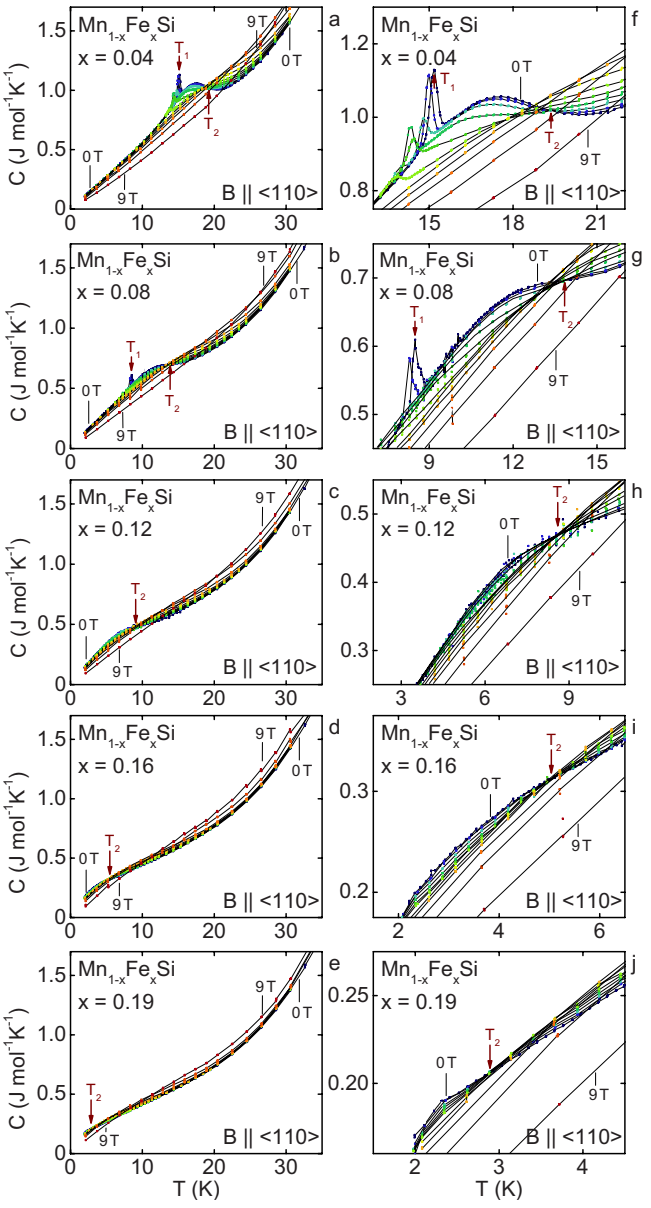

FIG. 30. (Color online) Specific heat of $Mn_{1-x}Fe_xSi$ as a function of temperature. Panels (a) through (e) show an overview up to 35 K. Panels (f) through (j) show a closeup view of the specific heat of $Mn_{1-x}Fe_xSi$ in the vicinity of the magnetic phase transition highlighting the sharp spike at T_1 and a Vollhardt invariance at T_2.

Debye temperature is not magnetic field dependent. This is supported by systematic measurements at 1.5, 3, and 9 T (not shown). Further, the rather high value of the Debye temperature and its invariance as a function of composition suggests that the crystal lattice is not dominantly involved in the suppression of the magnetic order. This supports the existence of a putative ferromagnetic quantum critical point masked by a quantum phase transitions at x_1 and the suppression of a Vollhardt invariance at x_2.

A canonical signature of quantum criticality is normally found in the electronic contribution to the specific heat. In a normal metal the specific heat is well described in Landau Fermi-liquid theory, where C_{el}/T represents a measure of the effective quasiparticle mass. A divergence of C_{el}/T due to

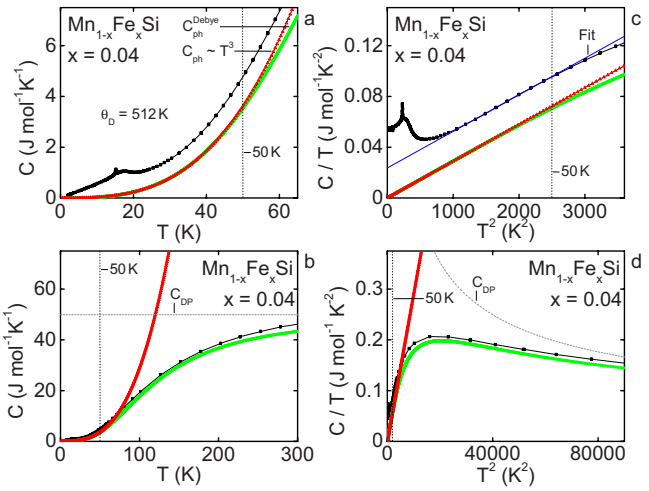

FIG. 31. (Color online) Typical data illustrating the estimate of the lattice contribution of the specific heat in MnSi, $Mn_{1-x}Co_xSi$, and $Mn_{1-x}Fe_xSi$. Data shown were recorded in $Mn_{1-x}Fe_xSi$ for $x = 0.04$. The experimental data are shown in black, the calculated contribution in the Debye model is shown in green; the cubic low-temperature approximation of the Debye contribution is shown in red. C_{DP} denotes the Dulong-Petit limit.

quantum critical fluctuations hence suggests a divergence of the effective mass, which, in turn, implies a breakdown of Fermi-liquid theory.

The electronic contribution to the specific heat divided by temperature, C_{el}/T, after subtraction of the lattice contribution (approximated by the cubic temperature dependence) is shown in Fig. 33 for MnSi, $Mn_{1-x}Fe_xSi$, and $Mn_{1-x}Co_xSi$. Data are shown for zero magnetic field and typical field values up to 9 T. At high temperatures essentially the same value of $C_{el}/T \approx 0.02$ J mol^{-1} K^{-2} is observed. For increasing magnetic fields this value slightly increases, as expected for a field-induced shift of magnetic entropy to high temperatures. For low doping concentrations and decreasing temperature C_{el}/T displays an increase with a pronounced maximum at the transition temperature, followed by an essentially temperature-independent specific heat at low temperatures. The contribution $\tilde{\gamma}_{fl}$ is remarkably large as compared with

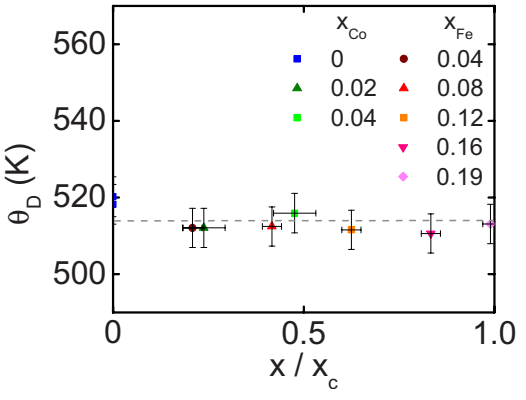

FIG. 32. (Color online) Debye temperature as a function of normalized concentration. The Debye temperature is essentially constant.

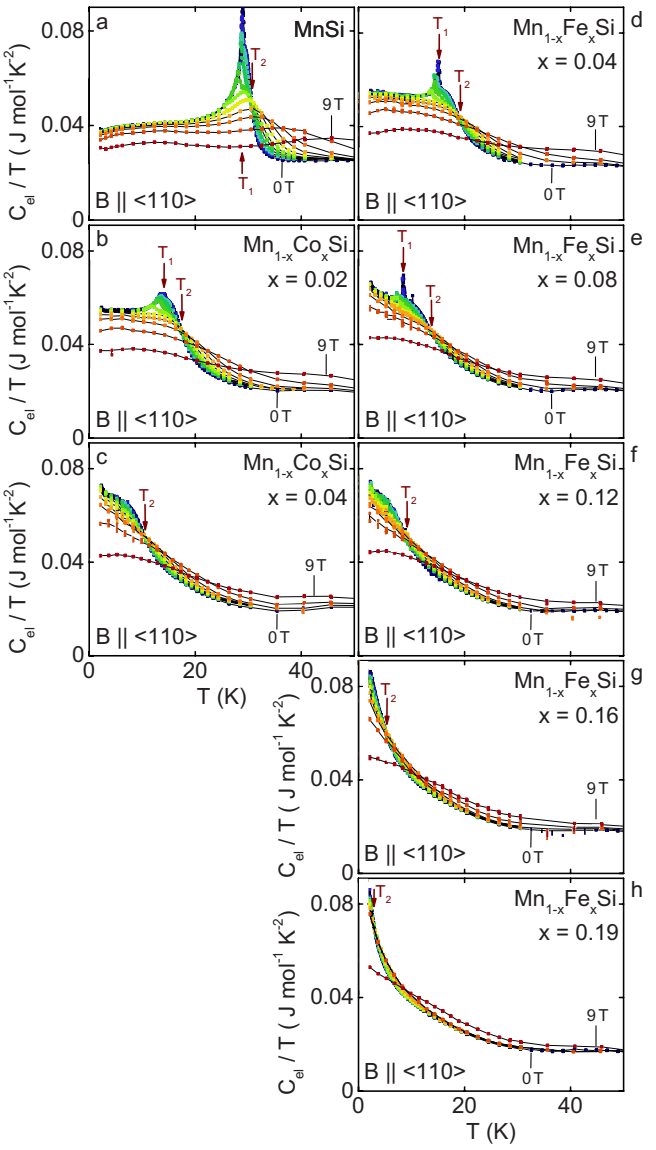

FIG. 33. (Color online) Temperature dependence of the electronic contribution of the specific heat divided by temperature, C_{el}/T, in MnSi, $Mn_{1-x}Co_xSi$, and $Mn_{1-x}Fe_xSi$ after subtraction of the lattice contribution calculated in a Debye model. For increasing magnetic field C_{el}/T is suppressed in the low-temperature limit and increases at high temperatures, characteristic of a shift of entropy to high temperatures.

normal Fermi liquids. At low temperatures the electronic contributions are thereby additionally enhanced as compared with the specific heat at high temperatures.

Toward the highest doping concentrations C_{el}/T increases monotonically with decreasing temperature. Magnetic field causes a suppression at low temperatures, where we find a linear increase with decreasing temperature for intermediate fields and the highest Co and Fe concentration studied. This clearly establishes that the increase in C_{el}/T is magnetic in origin.

The increase in C_{el}/T is unusual both quantitatively and qualitatively. Quantitatively the size of the electronic contribution is amongst the largest observed in any *d*-electron system so far, reaching in excess of 80 mJ mol^{-1} K^{-2}. Qualita-

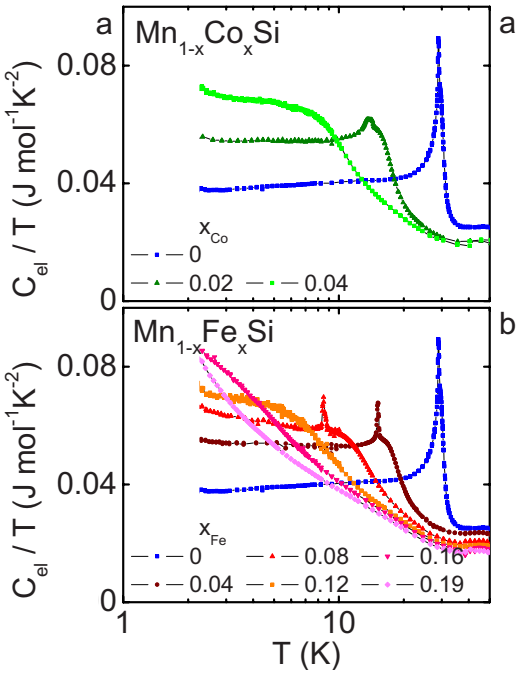

FIG. 34. (Color online) Electronic contribution of the specific heat divided by temperature versus temperature on a logarithmic scale. (a) Zero-field data for MnSi and $Mn_{1-x}Co_xSi$. (b) Zero-field data for MnSi and $Mn_{1-x}Fe_xSi$.

tively, as the critical concentration under Co or Fe doping is approached there is an increasingly wide range of an essentially logarithmic increase (Fig. 34). In fact, for $Mn_{1-x}Fe_xSi$ with $x=0.19$ this logarithmic increase extents over nearly an order of magnitude down to the lowest temperatures measured. Even though these data are recorded in zero field this is perfectly consistent with ferromagnetic quantum criticality. However, as concerns the nature of the quantum critical fluctuations one might expect them to be dominated by a ferromagnetic part, while the effects of the DM interactions assume a rather small spectral weight.

It is also instructive to plot the extrapolated zero-temperature contribution of the electronic specific heat as a function of normalized composition. As shown in Fig. 35 the extrapolated full electronic part, denoted as $\tilde{\gamma}_0$ increases toward the critical concentration. Extrapolating the electronic contribution seen at high temperatures, which is independent of temperature and denoted as $\tilde{\gamma}_{\mathrm{fl}}$, only decreases slightly.

Here a few words of caution are in place. First, experimentally nearly all quantum critical systems display data that can be fitted by a logarithmic divergence of C_{el}/T over at least a small temperature range, i.e., the specific heat tends to be insensitive to the precise nature of the quantum critical point. Second, the data presented here have not been measured sufficiently low in temperature to be conclusive beyond doubt. Future studies down to millikelvin temperatures will have to establish, if this logarithmic divergence indeed continues down to the lowest temperatures as we suggest. In summary our specific-heat data clearly support the formation of an underlying ferromagnetic quantum critical point as the magnetic transition temperature collapses to zero for $x \rightarrow x_c$.

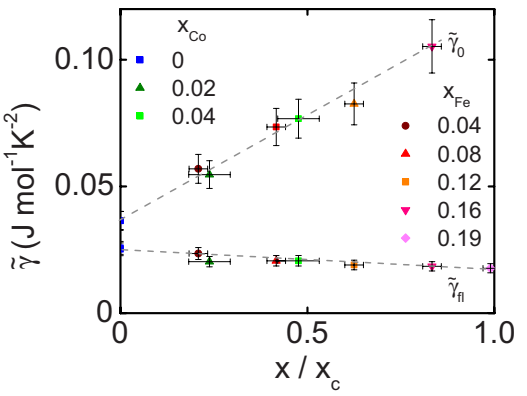

FIG. 35. (Color online) Extrapolated zero-temperature value of C_{el}/T denoted as $\tilde{\gamma}_0$ and the high-temperature contribution $\tilde{\gamma}_{\mathrm{fl}}$ observed well above T_c as a function of normalized concentration x/x_c.

B. Discussion of the specific heat

While conventional (thermal) phase transitions are driven by a reduction in entropy, this is not the case for quantum phase transitions. It is therefore interesting to consider the temperature versus entropy landscape when approaching the critical concentration x_c.

We have used the measured electronic contribution to the specific heat to obtain an estimate of the electronic part of the entropy $S_{\mathrm{el}}(T)=\int_0^T C_{\mathrm{el}}/T' dT'$. For the integration the temperature dependence of C_{el}/T was extrapolated linearly to zero, where we find the entropy to be insensitive to the precise extrapolation chosen. Shown in Fig. 36(a) is the electronic contribution to the specific heat (red data points). Subtracting the contribution at high temperatures (horizontal line above ~30 K) the contribution to C_{el}/T associated with the magnetic order may be obtained (purple data points). Shown in Fig. 36(b) is the associated entropy of the various contributions versus temperature, where the red and purple curves correspond to the total electronic and magnetic contributions, respectively.

For increasing temperature the full electronic contribution to the entropy increases monotonically and reaches a value around ~30% of R ln 2 at 50 K. In comparison, the magnetic entropy is essentially constant above ~30 K with a value of 12% R ln 2. This rather small entropy release and the tiny signature at the magnetic phase transition is a key characteristic of weak itinerant-electron magnetism, that reflects an abundance of soft spin fluctuations.

We have applied the same analysis to all $Mn_{1-x}Fe_xSi$ and $Mn_{1-x}Co_xSi$ compositions studied in this paper as shown in Fig. 37. Overall there is essentially no (dramatic) change in behavior for $x \rightarrow x_c$. In passing we note that the slight reduction in the entropy at high temperatures with increasing composition originates in the slight reduction in the high-temperature part of C_{el}/T (cf. $\tilde{\gamma}_{\mathrm{fl}}$ in Fig. 35). When approaching the critical concentration the entropy is already released at lower temperatures. This is summarized in Fig. 38 where isothermal lines of entropy are shown as a function of normalized composition. The contour lines suggest that quantum critical behavior emerges gradually over a wide

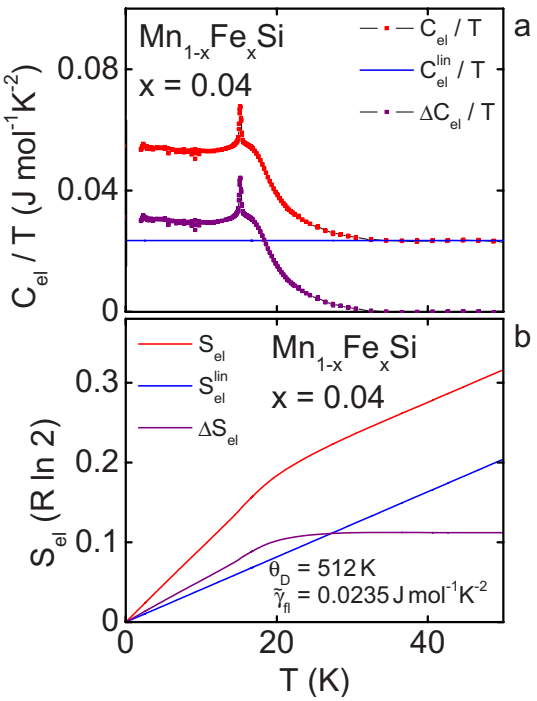

FIG. 36. (Color online) (a) Electronic specific heat divided by temperature of $Mn_{1-x}Fe_xSi$ for $x=0.04$, where red data points show the data after subtraction of the lattice contribution. At high temperatures the data are constant in temperature. Data shown in purple represent the low-temperature part after subtraction of the electronic contribution at high temperature. (b) Entropy as calculated for the three electronic contributions to the specific heat shown in (a).

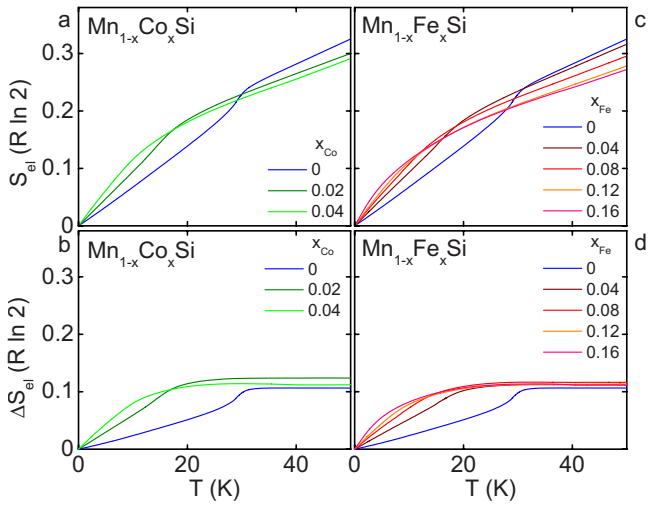

FIG. 37. (Color online) (a) Electronic part of the entropy of MnSi and $Mn_{1-x}Co_xSi$ as a function of temperature. (b) Magnetic part of the entropy of MnSi and $Mn_{1-x}Co_xSi$ as a function of temperature, i.e., after subtraction of the electronic contribution observed at high temperatures. (c) Electronic part of the entropy of MnSi and $Mn_{1-x}Fe_xSi$ as a function of temperature. (d) Magnetic part of the entropy of MnSi and $Mn_{1-x}Fe_xSi$ as a function of temperature, i.e., after subtraction of the electronic contribution observed at high temperatures.

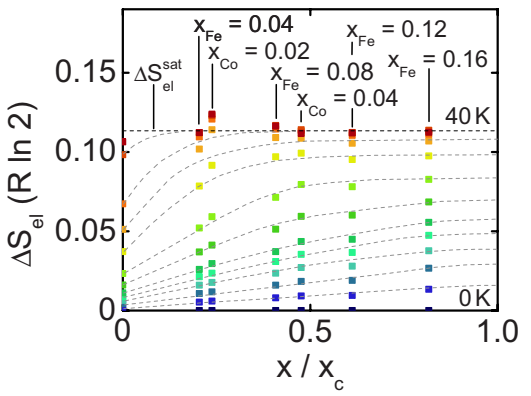

FIG. 38. (Color online) Isothermal magnetic entropy released as a function of normalized concentration for different temperatures.

range of x, rather than being confined to the immediate vicinity of x/x_c. This suggests that the specific heat may be rather insensitive to differences between x_1 and x_2, which are both close to x_c.

For each concentration magnetic field suppresses the electronic entropy at low temperatures thereby shifting the release of entropy to high temperatures (Fig. 39). At the high-

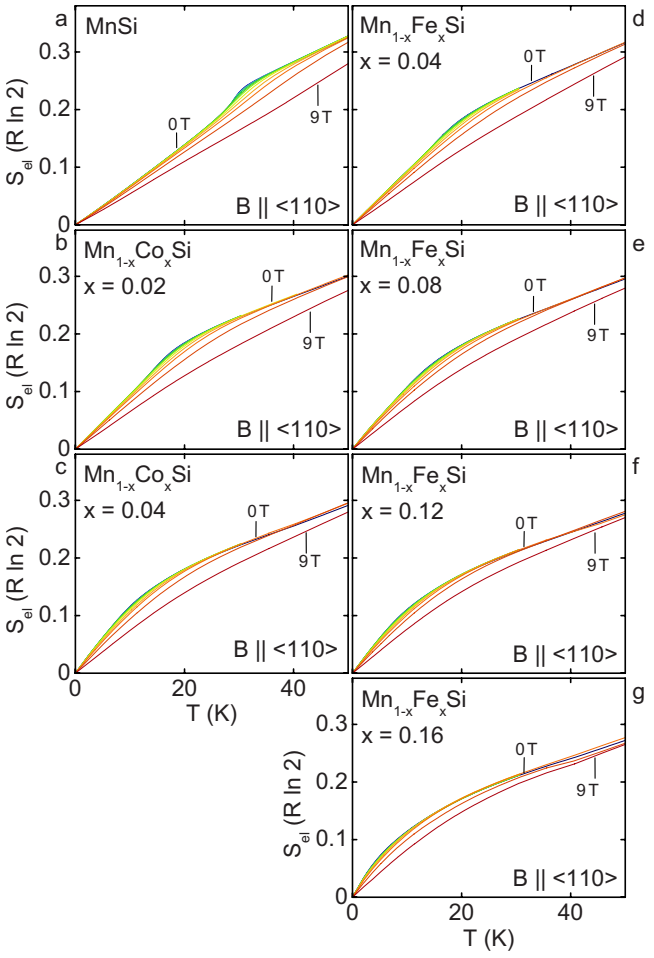

FIG. 39. (Color online) Electronic contribution to the entropy at various magnetic fields of MnSi, $Mn_{1-x}Co_xSi$, and $Mn_{1-x}Fe_xSi$ inferred from the electronic contribution to the specific heat.

est fields and lowest temperatures studied the electronic contribution to the entropy starts out with a linear temperature dependence over a wide range which turns into a superlinear temperature dependence for $x \to x_c$. This superlinear dependence reflects the increase in C_{el}/T with decreasing temperature shown in Fig. 33.

VII. CONCLUSIONS

Our studies of the magnetization, ac susceptibility, and specific heat of single-crystal $Mn_{1-x}Fe_xSi$ and $Mn_{1-x}Co_xSi$ show that the properties of both compounds are essentially identical on a normalized composition scale x/x_c. The critical concentrations $x_c^{Fe}=0.192$ and $x_c^{Co}=0.084$ of $Mn_{1-x}Fe_xSi$ and $Mn_{1-x}Co_xSi$, respectively, differ by nearly a factor of two. A simple explanation for this difference may be sought in the difference of valence electrons of Fe and Co as compared with Mn, which will affect the density of states accordingly (Fig. 40).

In zero magnetic field both compounds consistently suggest the existence of a putative quantum phase transition at a concentration x_1 associated with the suppression of the helical transition at T_1 followed by the suppression of the Vollhardt invariance at T_2 above $x_2 > x_1$. Determination of the critical exponents of the temperature dependence of the ac susceptibility and specific heat at precisely x_1 and x_2 requires studies down to millikelvin temperatures planned for the future. For the parameter range studied so far we cannot distinguish differences of critical exponents at x_1 and x_2.

In an applied magnetic field the ferromagnetic properties of $Mn_{1-x}Fe_xSi$ and $Mn_{1-x}Co_xSi$ inferred from the magnetization are characteristic of an underlying ferromagnetic quantum critical point at $x_1 < x_c < x_2$. Quite likely the thermodynamic properties reported here are dominated by these ferromagnetic quantum critical fluctuations even for $B=0$. It may hence be difficult to establish any characteristics unambiguously of the zero-field QPTs. As we consider doped compounds an interesting aspect concerns thereby the role of quenched disorder, which is expected theoretically to stabilize ferromagnetic quantum criticality.[12]

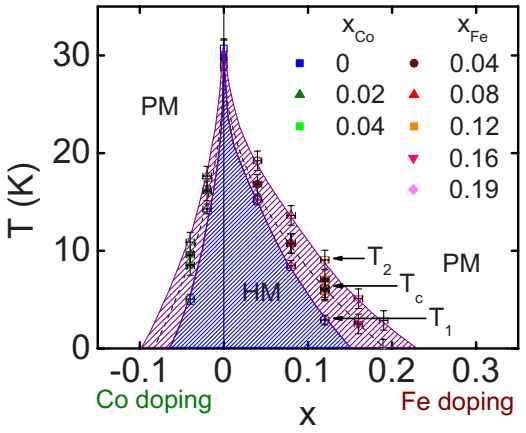

FIG. 40. (Color online) Temperature versus concentration phase diagram of $Mn_{1-x}Co_xSi$ (to the left) and $Mn_{1-x}Fe_xSi$ (to the right). The suppression of the extrapolated ferromagnetic transition is encompassed by the suppression of the helimagnetic transition and the onset of the intermediate regime, suggesting the possible existence a quantum phase transition at the border of a ferromagnetic quantum critical point followed by a zero-temperature Vollhardt point.

The evidence for quantum criticality in $Mn_{1-x}Fe_xSi$ and $Mn_{1-x}Co_xSi$ reported in this paper contrasts high-pressure studies in pure MnSi, where no quantum critical points have been found. Understanding the difference between pressure and compositional tuning of the magnetic properties of MnSi will, no doubt, provide important insights in the long-standing puzzle of the non-Fermi-liquid resistivity in MnSi at high pressures, as well as spin textures with nontrivial topology.

ACKNOWLEDGMENTS

We wish to thank B. Russ for assistance with the experiments and T. Adams, P. Böni, F. Jonietz, S. Mühlbauer, S. Legl, G. G. Lonzarich, R. Ritz, and A. Rosch for discussions. Financial support through DFG Transregio TRR 80 and DFG Forschergruppe FOR 960 are gratefully acknowledged.

*christian.pfleiderer@frm2.tum.de

[1] G. G. Lonzarich and L. Taillefer, J. Phys. C **18**, 4339 (1985).
[2] T. Moriya, *Spin Fluctuations in Itinerant Electron Magnetism*, Solid-State Sciences Vol. 56 (Springer, Berlin, New York, 1985).
[3] G. G. Lonzarich, J. Magn. Magn. Mater. **45**, 43 (1984).
[4] G. G. Lonzarich, J. Magn. Magn. Mater. **54-57**, 612 (1986).
[5] J. D. Thompson, Z. Fisk, and G. G. Lonzarich, Physica B **161**, 317 (1989).
[6] M. Uhlarz, C. Pfleiderer, and S. M. Hayden, Phys. Rev. Lett. **93**, 256404 (2004).
[7] C. Pfleiderer and A. D. Huxley, Phys. Rev. Lett. **89**, 147005 (2002).
[8] P. G. Niklowitz, F. Beckers, G. G. Lonzarich, G. Knebel, B. Salce, J. Thomasson, N. Bernhoeft, D. Braithwaite, and J. Flouquet, Phys. Rev. B **72**, 024424 (2005).
[9] S. Barakat, D. Braithwaite, P. Alireza, K. Grube, M. Uhlarz, J. Wilson, C. Pfleiderer, J. Flouquet, and G. G. Lonzarich, Physica B **359-361**, 1216 (2005).
[10] J. Schmalian and M. Turlakov, Phys. Rev. Lett. **93**, 036405 (2004).
[11] T. Vojta, D. Belitz, R. Narayanan, and T. Kirkpatrick, Europhys. Lett. **36**, 191 (1996).
[12] D. Belitz, T. R. Kirkpatrick, and T. Vojta, Phys. Rev. Lett. **82**, 4707 (1999).
[13] N. R. Bernhoeft (private communication).
[14] P. E. Bommer and J. J. M. Franse, in *Ferromagnetic Materials*, edited by K. H. J. Buschow and E. P. Wohlfarth (North-Holland, Amsterdam, 1988), Vol. 4, Chap. 3, pp. 211–308.
[15] M. Nicklas, M. Brando, G. Knebel, F. Mayr, W. Trinkl, and A. Loidl, Phys. Rev. Lett. **82**, 4268 (1999).

[16] M. Brando, W. J. Duncan, D. Moroni-Klementowicz, C. Albrecht, D. Grüner, R. Ballou, and F. M. Grosche, Phys. Rev. Lett. **101**, 026401 (2008).
[17] D. Moroni-Klementowicz, M. Brando, C. Albrecht, W. J. Duncan, F. M. Grosche, D. Grüner, and G. Kreiner, Phys. Rev. B **79**, 224410 (2009).
[18] R. Narayanan, T. Vojta, D. Belitz, and T. R. Kirkpatrick, Phys. Rev. B **60**, 10150 (1999).
[19] S. S. Saxena *et al.*, Nature (London) **406**, 587 (2000).
[20] A. D. Huxley, I. Sheikin, E. Ressouche, N. Kernavanois, D. Braithwaite, R. Calemczuk, and J. Flouquet, Phys. Rev. B **63**, 144519 (2001).
[21] D. Aoki, A. Huxley, E. Ressouche, D. Braithwaite, J. Flouquet, J.-P. Brison, E. Lhotel, and C. Paulsen, Nature (London) **413**, 613 (2001).
[22] F. Lévy, I. Sheikin, B. Grenier, and A. D. Huxley, Science **309**, 1343 (2005).
[23] C. Pfleiderer, Rev. Mod. Phys. **81**, 1551 (2009).
[24] Y. Ishikawa, Y. Noda, C. Fincher, and G. Shirane, Phys. Rev. B **25**, 254 (1982).
[25] Y. Ishikawa, Y. Noda, Y. J. Uemura, C. F. Majkrzak, and G. Shirane, Phys. Rev. B **31**, 5884 (1985).
[26] I. E. Dzyaloshinsky, Sov. Phys. JETP **5**, 1259 (1957).
[27] T. Moriya, Phys. Rev. **120**, 91 (1960).
[28] I. E. Dzialoshinskii, Sov. Phys. JETP **19**, 960 (1964).
[29] H. Z. Cummins, Phys. Rep. **185**, 211 (1990).
[30] K. Motoya, H. Yasuoka, Y. Nakamura, and J. H. Wernick, Solid State Commun. **19**, 529 (1976).
[31] Y. Ishikawa, K. Tajima, D. Bloch, and M. Roth, Solid State Commun. **19**, 525 (1976).
[32] S. Kusaka, K. Yamamoto, T. Komatsubara, and Y. Ishikawa, Solid State Commun. **20**, 925 (1976).
[33] P. Bak and M. H. Jensen, J. Phys. C **13**, L881 (1980).
[34] O. Nakanishi, A. Yanase, A. Hasegawa, and M. Kataoka, Solid State Commun. **35**, 995 (1980).
[35] M. Tanaka, H. Takayoshi, M. Ishida, and Y. Endoh, J. Phys. Soc. Jpn. **54**, 2970 (1985).
[36] M. Ishida, Y. Endoh, S. Mitsuda, Y. Ishikawa, and M. Tanaka, J. Phys. Soc. Jpn. **54**, 2975 (1985).
[37] Y. Ishikawa and M. Arai, J. Phys. Soc. Jpn. **53**, 2726 (1984).
[38] S. V. Grigoriev, S. V. Maleyev, A. I. Okorokov, Yu. O. Chetverikov, P. Boni, R. Georgii, D. Lamago, H. Eckerlebe, and K. Pranzas, Phys. Rev. B **74**, 214414 (2006).
[39] M. Janoschek, F. Bernlochner, S. Dunsiger, C. Pfleiderer, P. Böni, B. Roessli, P. Link, and A. Rosch, Phys. Rev. B **81**, 214436 (2010).
[40] B. Lebech, *Recent Advances in Magnetism of Transition Metal Compounds* (World Scientific, Singapore, 1993), p. 167.
[41] B. Lebech, P. Harris, J. S. Pedersen, K. Mortensen, C. I. Gregory, N. R. Bernhoeft, M. Jermy, and S. A. Brown, J. Magn. Magn. Mater. **140-144**, 119 (1995).
[42] S. V. Grigoriev, S. V. Maleyev, A. I. Okorokov, Y. O. Chetverikov, and H. Eckerlebe, Phys. Rev. B **73**, 224440 (2006).
[43] The explanation offered in Ref. 42 for a single helical modulation perpendicular to the applied magnetic field is based on the existence of a gap in the excitation spectrum of cubic helimagnets proposed in Ref. 104. Since the existence of this gap contradicts the Goldstone theorem, we believe that the theoretical explanation is incorrect. See also Ref. 39.
[44] C. Pfleiderer, D. Reznik, L. Pintschovius, H. v. Löhneysen, M. Garst, and A. Rosch, Nature (London) **427**, 227 (2004).
[45] F. Jonietz, S. Mühlbauer, C. Pfleiderer, A. Neubauer, R. Georgii, P. Böni, T. Adams, R. Duine, K. Everschor, M. Garst, and A. Rosch (unpublished).
[46] S. Mühlbauer, B. Binz, F. Jonietz, C. Pfleiderer, A. Rosch, A. Neubauer, R. Georgii, and P. Böni, Science **323**, 915 (2009).
[47] A. Neubauer, C. Pfleiderer, B. Binz, A. Rosch, R. Ritz, P. G. Niklowitz, and P. Böni, Phys. Rev. Lett. **102**, 186602 (2009).
[48] W. Münzer *et al.*, Phys. Rev. B **81**, 041203 (2010).
[49] C. Pfleiderer *et al.*, J. Phys.: Condens. Matter **22**, 164207 (2010).
[50] X. Z. Yu, Y. Onose, N. Kanazawa, J. H. Park, J. H. Han, Y. Matsui, N. Nagaosa, and Y. Tokura, Nature (London) **465**, 901 (2010).
[51] C. Pfleiderer and A. Rosch, Nature (London) **465**, 880 (2010).
[52] S. Doniach and S. Engelsberg, Phys. Rev. Lett. **17**, 750 (1966).
[53] K. K. Murata and S. Doniach, Phys. Rev. Lett. **29**, 285 (1972).
[54] J. A. Hertz, Phys. Rev. B **14**, 1165 (1976).
[55] A. J. Millis, Phys. Rev. B **48**, 7183 (1993).
[56] C. Pfleiderer, R. H. Friend, G. G. Lonzarich, N. R. Bernhoeft, and J. Flouquet, Int. J. Mod. Phys. B **7**, 887 (1993).
[57] C. Pfleiderer, G. J. McMullan, S. R. Julian, and G. G. Lonzarich, Phys. Rev. B **55**, 8330 (1997).
[58] C. Pfleiderer, S. R. Julian, and G. G. Lonzarich, Nature (London) **414**, 427 (2001).
[59] C. Pfleiderer, D. Reznik, L. Pintschovius, and J. Haug, Phys. Rev. Lett. **99**, 156406 (2007).
[60] C. Pfleiderer, J. Low Temp. Phys. **147**, 231 (2007).
[61] U. K. Rößler, A. N. Bogdanov, and C. Pfleiderer, Nature (London) **442**, 797 (2006).
[62] S. Tewari, D. Belitz, and T. R. Kirkpatrick, Phys. Rev. Lett. **96**, 047207 (2006).
[63] B. Binz, A. Vishwanath, and V. Aji, Phys. Rev. Lett. **96**, 207202 (2006).
[64] B. Binz and A. Vishwanath, Phys. Rev. B **74**, 214408 (2006).
[65] I. Fischer, N. Shah, and A. Rosch, Phys. Rev. B **77**, 024415 (2008).
[66] C. Pfleiderer, P. Böni, T. Keller, U. K. Rößler, and A. Rosch, Science **316**, 1871 (2007).
[67] Y. J. Uemura *et al.*, Nat. Phys. **3**, 29 (2007).
[68] A recent μSR study reports that there is no magnetic phase separation in MnSi under pressure (Ref. 105). Unfortunately the statements of good experimental conditions made in this paper are misleading. For instance, the sample quality with a residual resistivity ratio of 40, studied in Ref. 105, is much lower than for any of the samples studied in Refs. 44, 56–58, 60, 66, and 92, which range between 100 and 500. The absence of phase separation reported in Ref. 105 may be readily explained in terms of pinning and defects due to the low sample quality. Moreover, the pressure conditions reported in Ref. 105 are at best identical to those used in Refs. 44, 56–58, 60, 66, and 92, where a variety of different pressure transmitters including those used in Ref. 105 were employed. The use of Pb and In as pressure gauges suggests that the pressure values given in Ref. 105 are overestimated by up to 2 kbar. Finally, it is neither mentioned nor cited in Ref. 105 that Refs. 44, 56–58, 60, 66, and 92 report *consistent* evidence for phase separation in different samples of better quality using several different techniques, notably elastic neutron scattering, (Ref. 44) Larmor diffraction, (Ref. 66) and μSR (Ref. 67) as discussed in Ref. 49.

[69] A. Miyake, A. Villaume, Y. Haga, G. Knebel, B. Salce, G. Lapertot, and J. Flouquet, J. Phys. Soc. Jpn. **78**, 044703 (2009).
[70] K. Motoya, H. Yasuoka, Y. Nakamura, and J. H. Wernick, J. Phys. Soc. Jpn. **44**, 1525 (1978).
[71] J. Beille, J. Voiron, and M. Roth, Solid State Commun. **47**, 399 (1983).
[72] E. Achu, H. Al-Kanani, J. Booth, M. Costa, and B. Lebech, J. Magn. Magn. Mater. **177-181**, 779 (1998).
[73] E. Bauer, A. Galatanu, R. Hauser, C. Reichl, G. Wiesinger, G. Zaussinger, M. Galli, and F. Marabelli, J. Magn. Magn. Mater. **177-181**, 1401 (1998).
[74] N. Manyala, Y. Sidis, J. F. DiTusa, G. Aeppli, D. P. Young, and Z. Fizk, Nature (London) **404**, 581 (2000).
[75] N. Manyala, Y. Sidis, J. F. DiTusa, G. Aeppli, D. P. Young, and Z. Fisk, Nature Mater. **3**, 255 (2004).
[76] N. Manyala, J. F. DiTusa, G. Aeppli, and A. P. Ramirez, Nature (London) **454**, 976 (2008).
[77] S. V. Grigoriev, V. A. Dyadkin, E. V. Moskvin, D. Lamago, T. Wolf, H. Eckerlebe, and S. V. Maleyev, Phys. Rev. B **79**, 144417 (2009).
[78] S. V. Grigoriev *et al.*, Phys. Rev. B **81**, 012408 (2010).
[79] C. Meingast, Q. Zhang, T. Wolf, F. Hardy, K. Grube, W. Knafo, P. Adelmann, P. Schweiss, and H. v. Löhneysen, in *Properties and Application of Thermoelectric Materials*, Proceedings of the NATO Advanced Research Workshop, Hvar, Croatia, 21–26 September 2008, edited by V. Zlatic and A. C. Hewson (Springer Science + Business Media B.V., Heidelberg, 2009), p. 261.
[80] A few years ago Vollhardt had pointed out that the specific heat of many correlated electron systems displays these invariant crossing points as a function of a control parameter (Ref. 81). The invariant crossing point in the specific heat is particularly well defined, when it coincides with a point of inflection in the susceptibility, i.e., $\partial^2\chi/\partial T^2=\partial^2\gamma/\partial B^2=0$ from which follows $\partial^2 C/\partial B^2=0$.
[81] D. Vollhardt, Phys. Rev. Lett. **78**, 1307 (1997).
[82] T. Adams, S. Mühlbauer, A. Bauer, A. Neubauer, R. Georgii, P. Böni, and C. Pfleiderer (unpublished).
[83] C. Franz, A. Bauer, A. Neubauer, and C. Pfleiderer (unpublished).
[84] A. Neubauer, J. Bœuf, A. Bauer, B. Russ, H. v. Löhneysen, and C. Pfleiderer (unpublished).
[85] D. Bloch, J. Voiron, V. Jaccarino, and J. H. Wernick, Phys. Lett. A **51**, 259 (1975).
[86] T. Sakakibara, H. Mollymoto, and M. Date, J. Phys. Soc. Jpn. **51**, 2439 (1982).
[87] M. Otero-Leal, F. Rivadulla, S. S. Saxena, K. Ahilan, and J. Rivas, Phys. Rev. B **79**, 060401 (2009).
[88] S. M. Stishov, Phys. Rev. B **80**, 136401 (2009).
[89] M. Otero-Leal, F. Rivadulla, S. S. Saxena, K. Ahilan, and J. Rivas, Phys. Rev. B **80**, 136402 (2009).
[90] K. Koyama, T. Goto, T. Kanomata, and R. Note, Phys. Rev. B **62**, 986 (2000).
[91] C. Thessieu, K. Kamishima, T. Goto, and G. Lapertot, J. Phys. Soc. Jpn. **67**, 3605 (1998).
[92] C. Thessieu, C. Pfleiderer, A. Stepanov, and J. Flouquet, J. Phys.: Condens. Matter **9**, 6677 (1997).
[93] M. Uhlarz, Ph.D. thesis, Universität Karlsruhe, 2004.
[94] C. Franz, C. Pfleiderer, A. Neubauer, M. Schulz, B. Pedersen, and P. Böni, J. Phys.: Conf. Ser. **200**, 012036 (2010).
[95] N. R. Bernhoeft (private communication).
[96] S. M. Stishov, A. E. Petrova, S. Khasanov, G. K. Panova, A. A. Shikov, J. C. Lashley, D. Wu, and T. A. Lograsso, Phys. Rev. B **76**, 052405 (2007).
[97] S. M. Stishov, A. E. Petrova, S. Khasanov, G. K. Panova, A. A. Shikov, J. C. Lashley, D. Wu, and T. A. Lograsso, J. Phys.: Condens. Matter **20**, 235222 (2008).
[98] D. Lamago, R. Georgii, C. Pfleiderer, and P. Böni, Physica B **385-386**, 385 (2006).
[99] D. Belitz, T. R. Kirkpatrick, and A. Rosch, Phys. Rev. B **73**, 054431 (2006).
[100] C. Pfleiderer, C. Thessieu, R. Calemczuk, G. Lapertot, J. Flouquet, D. Lamago, P. Böni, and G. G. Lonzarich (unpublished).
[101] C. Pfleiderer, J. Magn. Magn. Mater. **226-230**, 23 (2001).
[102] C. Pappas, E. Lelièvre-Berna, P. Falus, P. M. Bentley, E. Moskvin, S. Grigoriev, P. Fouquet, and B. Farago, Phys. Rev. Lett. **102**, 197202 (2009).
[103] S. V. Grigoriev, S. V. Maleyev, E. V. Moskvin, V. A. Dyadkin, P. Fouquet, and H. Eckerlebe, Phys. Rev. B **81**, 144413 (2010).
[104] S. V. Maleyev, Phys. Rev. B **73**, 174402 (2006).
[105] D. Andreica, P. Dalmas de Réotier, A. Yaouanc, A. Amato, and G. Lapertot, Phys. Rev. B **81**, 060412 (2010).